Received 11 July 2024; revised 24 August 2024; accepted 9 September 2024. Date of publication 16 September 2024; date of current version 22 November 2024.

Digital Object Identifier 10.1109/OJAP.2024.3462289

Recent Advances in Antennas for Biotelemetry and Healthcare Applications

RIQZA Y. KHATTAK[1] (Student Member, IEEE), QASIM Z. AHMED[1] (Member, IEEE), SULTAN SHOAIB[2] (Senior Member, IEEE), PAVLOS I. LAZARIDIS[1] (Senior Member, IEEE), AND TEMITOPE T. ALADE[3]

[1]Department of Engineering and Technology, School of Computing and Engineering, University of Huddersfield, HD1 3DH Huddersfield, U.K.
[2]Faculty of Arts, Computing and Engineering, Wrexham University, LL11 2AW Wrexham, U.K.
[3]School of Computing Science, Faculty of Science, University of East Anglia, Norwich Research Park, NR4 7TJ Norwich, U.K.

CORRESPONDING AUTHOR: R. Y. KHATTAK (e-mail: riqza.khattak@hud.ac.uk)

This work was supported in part by the Department of Engineering and Technology, School of Computing and Engineering, University of Huddersfield, U.K., and in part by the Erasmus+ programme of the European Union through the "Capacity building for Digital Health Monitoring and Care Systems in Asia (DigiHealth-Asia), 2021–2024" Project under Agreement 619193-EPP-1-2020-1-BE-EPPKA2-CBHE-JP.

ABSTRACT This paper provides a detailed examination of recent advancements in antenna design tailored specifically tailored for applications in biotelemetry and healthcare. It contains a detailed analysis of over 60 journal papers retrieved from the Institute of Electrical and Electronics Engineers (IEEE) database within the past five years. Each paper is briefly discussed, emphasizing its simulation and/or practical results. Furthermore, the paper draws conclusions based on various performance parameters, highlighting key shortcomings in existing literature designs, and identifying prerequisites for future high-performance antennas. Finally, the paper proposes a new antenna design positioned to surpass most of the antennas discussed herein. Tailored for the 5.8 GHz industrial, scientific, and medical (ISM) band, the proposed antenna boasts a compact footprint of 7.7×6 mm^2. The antenna possesses noteworthy performance metrics including a mean gain of 1.2 dB and an efficiency exceeding 51% when in direct contact with a body.

INDEX TERMS Implantable antennas, digital health, in–body and on–body antenna.

I. INTRODUCTION

WIRELESS sensing and detection have sparked interest among researchers worldwide in recent years. Digital health technologies have evolved that are promising in providing remote care and medicine delivery. Antennas are mandatory parts of any wireless communication system. The integration of antennas into implantable medical devices allows for continuous health tracking offering essential data for early detection and management of chronic illnesses. This seamless fusion of sensing technology with health platforms is transforming patient care by improving accessibility, cutting healthcare expenses, and enhancing outcomes. Designing antennas that function efficiently near the body presents challenges due to the complex absorbent nature of biological tissues. To achieve sensing it is essential to design antennas with good gain, low specific absorption rate (SAR), and optimal efficiency. Balancing these aspects poses a research hurdle in this field globally. Ongoing research aims to improve the performance and reliability of sensing and detection systems. Researchers have designed and tested different antenna designs for both in- and on-body applications. However, a key challenge in antenna areas is that they can maintain their performance in gain and efficiency when placed inside or under tissue layers. By tackling these challenges researchers can enhance the efficiency and effectiveness of healthcare delivery for antenna-related research.

This paper provides an in-depth review of diverse implantable and on-body antennas tailored for medical applications. This analysis utilizes over 60 journal papers sourced from the Institute of Electrical and Electronics Engineers (IEEE). These papers will be reviewed in terms

of geometry, resonance, and radiation performances. A comparative analysis will be conducted, examining the critical parameters such as gain, efficiency, SAR, antenna type, and frequency of operation. A new antenna design is proposed, and its performance is compared to the findings from these reviewed papers.

II. MEDICAL ANTENNAS

Numerous designs of antennas for on-body and implantable applications at different frequencies have been presented. Generally, different shapes and geometries are presented with various types of feeding mechanisms. A design of a broadband implantable loop antenna is presented in [1]. The design is composed of complementary split ring resonators (CSRRs). The antenna covers multiple frequency bands falling in the industrial, scientific, and medical (ISM) spectrum. The flexible antenna has a transmission range of 2m and is useful for small-sized cylindrical implants. Measurements of the presented antenna were conducted using a pork phantom that serves as an excellent heterogeneous medium. Simulating, the spacing of λ/4 is kept in the off-body direction. The gain achieved by the antenna with CSRRs in the simplified body is −26 dB at 0.403 GHz and −15 dB at 2.45 GHz whereas without CSRRs it is −27.9 dB at 0.403 GHz and −17.52 dB at 2.45 GHz. The radiation efficiency achieved with CSRRs in the simplified body is 0.12% at 403 MHz and 0.53% at 2.45 GHz whereas, without CSRRs it is 0.09% at 403 MHz and 0.46% at 2.45 GHz. The simulated radiation efficiency in the functional body model with CSRRs is 0.04% at 403 MHz and 0.53% at 2.45 GHz. The simulated peak gain achieved by the antenna with CSRRs is −36 dBi at 403 MHz and −19.8 dBi at 2.45 GHz. The main benefit is to minimize power absorption inside the body and to maximize impedance matching.

A circularly polarized (CP) implantable patch antenna is presented in [2] to overcome a narrow axial ratio (AR) bandwidth that occurs in the ISM spectrum. To design the antenna, a layer of cubic skin with the dimensions of 90 × 90 × 25.27 mm^3 is used. Three body models including scalp, cylindrical muscle, and three-layered phantoms are used to assess the antenna's sensitivity and suitability for practical use. The antenna consists of a center square slot and four slits with short pins having a diameter of 0.5mm. The bandwidth obtained during simulations is 150 MHz spanning from 2.35 to 2.50 GHz (6.2%), while the simulated AR ranges from 2.36 to 2.56 (8.13%), accompanied by a gain of −27.2 dBi in the boresight direction. The antenna employs polyvinyl chloride (PVC) as an insulation material for biocompatibility. The observed impedance bandwidth for all body models falls within the range of 2.4 to 2.48 GHz. Validation is conducted using skin-mimicking gel and minced pork to verify the performance of the implantable antennas. The measured radiation efficiency is 5.45% in the case of a gel whereas, in the case of pork, it is 5.69%. A wide 10% AR bandwidth obtained in the case of pork ranges from 2.38 to 2.63 GHz.

In [3], a coaxial dipole antenna is designed. The antenna has found application in orthopedics where it is used for passive sensing of object displacement and deflection. The design consists of two 85cm long coaxial cables, spaced 15mm apart to align with the three harmonic positions of highest sensitivity. A frame with a contact point is used to position the antenna against the target fractured bone, securing the cables in place. The antenna design underwent parametric tests, including plate placement and cable spacing, to optimize sensitivity. The frequency sweep and resonant frequencies were observed at 85, 179, and 275 MHz. The location of sensitivity was determined by local minima in the frequency plot, with the third harmonic showing substantial resonant frequency shifts. A second test was conducted on the cable spacing which demonstrated that sensitivity increases with the increase of cable spacing. It is desirable to increase spacing up to 40 mm, but it is restricted to do so because the design is intended to be used for sensing the deformation of the plate that is attached to a fractured bone. Two tests were conducted to evaluate the efficacy of the antenna: plate displacement and orthopedic plate compression, complemented by computational models. When the plate is displaced away from the antenna, there is an observed increase in frequency. Notably, a greater shift in resonant frequency is observed when using a double plate. For a 50mm displacement, the antenna exhibited a quality factor (QF) measurement of 400. Apparent resonant frequency (ARF) values through the inverse square model were determined to be 0.04 and 0.14 MHz for the single and double plate configurations, respectively. From the validation compression test, it was found that the resonant frequency and applied load had a linear relationship. A 500N load is applied to the acetal bar which produces a deflection in the plate through a tensile strain of 1353 $\mu\varepsilon\pm$ 6 $\mu\varepsilon$. This deflection of the plate leads to a decrease in the plate's ARF. Strain prediction by finite element simulation is $1340\mu\varepsilon \pm 58\mu\varepsilon$. The relative predicted deflection under the load is to be 0.58mm. The presented system can be used for tracking the healing process and is suitable for future diagnosis and health monitoring terminals.

A design of a compact Perylene-coated flexible antenna is presented [4]. The presented Wireless Local Area Network (WLAN)-based antenna is composed of meandered strips and a coupling patch. The design is flexible and completely insulated with a biocompatible Perylene-C coating making the antenna cost-effective and feasible for such applications. The Perylene-C film and the bending have insignificant effects on the S-parameters and the radiation pattern. The original WLAN antenna was tuned to resonate at 2.4 GHz under the implanted conditions. The measured gain of the antenna is −5.4 and −3.8 dBi at 2.4 and 5.8 GHz, respectively. The maximum radiation gain of the antenna under the skin without tuning is −12.9 dBi and enhances to 0.8 dBi after tuning.

Another design of an implantable antenna with enhanced gain is presented in [5] for ISM band biomedical applications. A coplanar waveguide (CPWG)-fed, compact,

and flexible antenna is demonstrated, consisting of two concentric rings of equal slot width of 0.5 mm with the outer radius of 3.5 mm and 2.5 mm. The design is fabricated on a 10 × 10 × 0.4 mm^3 Kapton polyimide substrate. The design can achieve a maximum gain of −12 dB whereas, the calculated efficiency lies between 2.5% and 5.6%. To enhance the gain a 2 × 2 array of metamaterial structure (MTM) with epsilon-very-large (EVL) is introduced as a superstrate. This leads to a 3 dB increase in the gain while maintaining it lightweight, compactness, flexibility, and wideband characteristics. The parameters of the fabricated antenna were determined by submerging the prototype in a single tissue-emulating gel and a loaf of chicken breast. The impedance bandwidth attained is approximately 57% and the peak averaged SAR value obtained is 124 W/kg.

A multiband high-frequency (HF) and ultra-high frequency (UHF) antenna system for simulation devices and neural recording is presented in [6]. The antenna is designed to sustain power over a long duration and can communicate with an external system using adequate bandwidth. The structure comprises of three layers, incorporating an internal ground plane and concealed vias. The implanted antenna is sandwiched on both the top and bottom layers of the stack, each covered with a 1-mm-thick layer of Teflon. The measured power transfer efficiency in the HF band stands at 17% and the UHF communication link exhibits a 38 dB insertion loss across the frequency range of 902 – 928 MHz.

A design of a multiband rectenna system for wireless transmission of data and power is presented in [7]. The design is aided by a rectifier and a compact planar inverted F-antenna (PIFA). The size of the presented antenna is 16 × 14 × 1.27 mm^3 with a slotted ground plane. The introduction of slits and or slots in the radiator allows the design to have a reduced size and dual-band operation. The implant depth of this presented antenna is 10 mm in muscle. In the case of a single-layered substrate, the bandwidth, and gain of antenna is 5.7% and −24.3 dB, respectively. At 915 MHz, the presented arm attached improves PIFA's directivity and radiation quality, resulting in a 6.2 dB increase in the antenna's received power at a transmission distance of 50 cm.

Reference [8] presents a millimeter-scale crystal-less transceiver designed for insertable smart pills operating within the medical implant communication system (MICS) band. The focus was to study electromagnetic (EM) absorption within the body. The phase tracking receiver offers coverage with a ±160 ppm frequency deviation. Both transmitter and receiver impedance matching, along with mode switching, are handled by a tunable matching network (TMN). A loop-back power detector with self-mixing is employed for dynamic calibration of antenna impedance variation across different positions and dietary conditions, thereby enhancing the power contour up to a 4.8 voltage standing wave ratio (VSWR). The transceiver system is developed in a 40nm complementary metal-oxide-semiconductor (CMOS) technology and takes 2mm^2 of space. In wireless measurements, the receiver sensitivity is 90 dBm with a liquid phantom, at 200Kbps data rate and 25 dBm EIRP.

Another design of the miniature antenna is designed for the MedRadio band and is shown in [9]. The antenna design presented has a volume of 12.5 ×12.5 ×1.27 mm^3 at a frequency of 403MHz. The size is reduced by 198 mm^3 (including superstrate) by incorporating meandering and shorting techniques. To assess the feasibility of the presented concept, a prototype is designed and tested in vitro. The peak realized gain is −32.49 dBi at a frequency of 403 MHz. Measured and simulated bandwidths are 7.26% and 6.15%, respectively. S_{11} of the presented antenna is −36.9 dB at 402 MHz. The maximum 1-g and 10-g average SARs under the assumption of 1 W input power are 192.59 W/kg and 36.23 W/kg, respectively. The permitted input power is limited to 8.31 and 55.20 mW, respectively, to satisfy IEEE standards.

In [10], a miniaturized annular-ring antenna with CP is introduced. Two stubs with open ends and rectangular slots are engraved at the inner edge of the ring to achieve CP and size reduction in the presented design. The central patch is also modified with a Z-shaped slot to improve the AR. All these techniques contribute towards the improvement of impedance matching. The complete design presented in this work occupies the dimensions of 120.69 mm^3. The −10 dB impedance bandwidth ranges from 2.31 to 2.51 GHz (8.3%) in simulations whereas, the measured bandwidth extends from 2.39 to 2.68 GHz (11%). The 3dB AR bandwidth is reported as 2.49% in simulations. The design achieves acceptable SAR values, making it suitable for implantable applications.

The implantable antenna in [11], is a miniaturized CP design aimed at subcutaneous real-time glucose monitoring within the ISM band. The antenna incorporates four slots in the shape of 'C' and a CSRR to achieve effective miniaturization. CP is attained by adjusting the slits of the CSRR. The simulations revealed an impedance bandwidth of 12.2% ranging from 2.32 to 2.62 GHz with the highest gain of −17 dBi. The 3-dB AR bandwidth is documented at 2.4% (2.42–2.48 GHz), complemented by a broad beamwidth of 140°. In practical testing within a pork slab, the measured impedance bandwidth expands to 13% (2.31–2.63 GHz) with S_{11} values below −10 dB. The calculated link margin suggests reliable communication within a 10-meter range in free space.

A biotelemetry system ISM bands are presented in [12]. The device occupies a volume of 434.72 mm^3 which includes batteries and electronic circuitry. The antenna integrated into this compact device boasts a volume of 9.8 mm^3, with dimensions of 7 mm in length and width, and a height of 0.2 mm. The peak gain values for the antenna observed in the heterogenous environment are −28.04 dBi at 915 MHz and −23.01 dBi at 2450 MHz. For a homogenous environment, the gain is −28.94 dBi at 915 MHz and −23.06 dBi at 2450 MHz. Practical validation involves

submerging the complete system involving the antenna and its related circuitry in a 3-dimensional (3D) saline head. To evaluate the in-body communication reach, a link budget estimate is employed, considering various data rates whereby keeping the input power capacity to −16 dBm (25μW). SAR values for the 1g and 10g standards are measured at 730.07 and 89.70 W/kg at 915 MHz, respectively, with an input power of 1 W. The SAR values at 2.45 GHz are 591.4 W/kg for 1g of tissue and 82.7 W/kg for 10g of tissue. The achieved bandwidth for the presented antenna is 560 MHz.

In a separate study [13], a 2.45 GHz ISM based multiple input multiple output (MIMO) antenna with a small size is introduced to address multipath fading and ensure an adequate transmission rate. To ensure maximum isolation, the MIMO antenna system employs techniques such as slots in the main element and passive microstrip lines in the ground plane. EM band gaps are used for additional improvement in the isolation. MIMO antenna has a compact footprint of 18.5 × 18.5 × 1.27 mm^3. Impedance matching in the three-layer phantom provided a significant bandwidth of 18.64% from 2.14 to 2.58 GHz with a maximum gain of −15.18 dBi. The simulated envelope correlation coefficient calculations suggest an isolation better than −15 dB. An experiment involving a fresh pork slab is conducted to assess the antenna's suitability for biomedical telemetry, and the link budget.

A multiband miniaturized antenna for battery-powered implantable devices is presented in [14]. The design operates in the 915 MHz and 2.45 GHz ISM bands. Rogers ULTRALAM liquid crystalline polymer material with a permittivity of 2.9 and tanδ of 0.0025 is utilized for both substrate and superstrate. With the thicknesses of 0.1 mm, the design achieves a reduced volume of 7 × 7.2 × 0.2 mm^3. The reviewed antenna exhibits the highest gain of −28.44 dBi at 928 MHz and −25.65 dBi at 2.45 GHz, specifically in a homogeneous skin phantom. The peak SAR values fall within the safe range, adhering to the protection requirements outlined in IEEE C95.1-1999 and C95.1-2005 standards. Emitting omnidirectional radiation, the flower-shaped antenna proves suitable for applications in gastro procedures and skin implantations. Impressive data rates are achieved, with rates of 7 Kb/s at 928 MHz and 78 Mb/s at 2.45 GHz, covering transmission ranges of more than 6 m and 1.5 m, respectively. Experimental measurements involve the substitution of the fabricated prototype into a head phantom containing a saline solution. SAR calculations indicate that the maximum allowable power for implantable applications exceeds 25 μW.

Design for bio-telemetry applications is presented in [15]. This work proposes a miniaturized triple-band implantable antenna system that functions in the ISM and the midfield bands. The presented antenna system consists of two implantable modules of which one is capsule type with a volume of 647 mm^3 and is for deep tissues whereas, the other is flat type for skin with a volume of 425.6 mm^3. The size reduction is attained by utilizing various techniques such as bending the structure of the radiating patch, placing a shorting pin between the ground plane and the radiating patch, and incorporating an open-end ground slot. The simulated bandwidth of the presented antennas in the ISM 902 MHz band is 8.7% whereas, that at ISM 2.45 GHz band is 7.3%. Likewise, in the midfield band, the bandwidth achieved is 8.2%. The testing of the antenna is carried out in a saline solution. The practical percentage bandwidth obtained is 14.7% at the lower ISM band whereas, at the upper ISM band it is 24.8%. Similarly, in the midfield band, it is 13.1%. Additionally, a link budget is also computed at various data rates to determine the data telemetry range. Furthermore, a link budget for far-field communication of an in-body implant with an external base station is also determined considering microelectronics, sensors, and batteries being integrated with the antenna system. To simulate for various applications implantation is done into different environment tissues such as stomach, large intestine, colon, heart, and scalp. The maximum gain of the presented antenna in the case of the human scalp is −26.4, −23, and −20.47 dB at 915, 1900, and 2450 MHz respectively.

The design, modeling, and testing of a low-profile rectenna system for RF energy harvesting in leadless pacemakers is presented in [16]. The rectenna system under discussion is specifically designed for operation with ultra-low radio frequency (RF) input power. In simulations, the system demonstrates significant power capture, reaching nearly 20 dBm when positioned 50 mm away from the body. The antenna structure presented in this study is a miniature spiral planar inverted-F antenna (PIFA) with CP, operating at a frequency of 673 MHz. Experimental results show that the antenna achieves a 10 dB bandwidth of 15 MHz while maintaining an AR smaller than 3 dB both within and outside of sheep fat tissue. Two different rectifiers are manufactured and systematically compared to identify the most suitable option, especially under ultra-low RF input power conditions. The study focuses on two Schottky diode rectifiers, and evaluates their performance. To enhance the power conversion, a matching circuitry is implemented. The housing for the rectenna system is a cylindrical structure with a radius of 5 mm and a height of 3.2 mm. With a −20 dBm input power and a 10kΩ load, the rectenna's efficiency is 40% and the direct current (DC) output voltage obtained is approximately 0.2V. The reflection coefficient and the gain of the presented antenna at 675 MHz are −19 dB and −15.37 dBi, respectively. For an input power of 27 dBm, the maximum achieved SAR is 0.078 which is safe for a human body.

Reference [17] introduces a wireless sensor designed for glucose monitoring, focusing on long-range capabilities. The implantable biosensor features a fully passive and miniaturized circuit, comprising a 16 mm^3 inductor-capacitor (LC) tank resonator. Constructed with a rectangular metallic conductive plate and a rectangular spiral coil on an FR4 substrate dielectric material, the passive LC sensor is designed to be inserted beneath the human skin. Testing conducted

in skin and fat phantom tissues, as well as with different glucose concentrations in deionized water and human serum albumin, demonstrated a linear relationship between resonant frequency and glucose concentration within the range of 0–500 mg/dL. The sensor exhibited a sensitivity of approximately 150 kHz/(mg/dL), and reliable measurements were achieved at distances up to 10 mm between the reader and the sensor. The presented device was created to be extremely thin, allowing for simple placement under the skin. The glucose level can be constantly tracked without inducing discomfort after it is injected minimizing the need to prick a human finger.

A differentially fed multiband design for biotelemetry functions is discussed in [18]. The presented planar antenna operates in the MICS and the ISM bands. The lower band's estimated bandwidth is 389–419 MHz (7.4%), whereas the upper band's bandwidth is 2.395–2.563 GHz (6.6%). A differentially fed lightweight dual-band configuration is obtained using symmetric meandered strips and shorting pins, with a prototype volume of 642.62 mm3. The strip must be secured from close interaction with the semiconducting bio-fluid by using a superstrate. The antenna, positioned at a depth of 4 mm within a skin-mimicking material of 1000 mL, exhibits simulated far-field gains of −36.7 and −27.1 dBi at 402 and 2400 MHz. Additionally, the simulated CP discriminations in the boresight direction are 34.9 and 35.7 dBs at 402 and 2400 MHz, respectively. Notably, the coupling is higher in the ISM band compared to the MICS band due to the larger gains in the ISM band. The compact size and dual-band functionality of this antenna make it well-suited for integration into implantable biotelemetric devices, particularly for connecting to differential circuits. The simulated 1-g averaged SAR values comply with the IEEE regulation. The 1g averaged SAR values are 832 W/kg and 690 W/kg at 402 MHz and 2.4 GHz respectively.

A design of a wireless rectenna-based pacemaker is presented in [19]. A leadless pacing system designed for direct implantation into the heart, utilizing wireless RF energy for its power source was presented. The system is comprised of an implantable rectenna, a charging circuitry, and the pacing electronics. An external wearable transmit-antenna array (TA) was designed for the transmission of EM energy into the deep tissues. In a sensitive animal investigation using ovine models, the leadless pacing (LP) was successfully inserted at the left ventricular apex through thoracotomy. The fabricated LP received its power wirelessly from the wearable TA, demonstrating an effective leadless pacing as evidenced by the in vivo ECG results. The measured gain for the antenna is 0.64 dB. The average computed SAR is 0.29 W/kg at the frequency of 924 MHz, the output power is 10 dBm and the efficiency is 65%.

In [20], an ultrawideband antenna system of compact size has been introduced, featuring consistent impedance matching. The presented antenna is characterized by its compact size of 28.85 mm^3 and is meticulously designed to mitigate detuning issues arising from variations in implantation situations and coupling with the device's electronics. The antenna and the associated devices are developed within a homogeneous muscle box, containing batteries, sensors, and the antenna, all enclosed in a biocompatible housing. Utilizing 3D printing technology, the antenna and devices are fabricated for practical implementation. The setup includes the fabricated antenna, circuit, and 3D-printed flat and capsule-type devices. In simulations and measurements, a substantial bandwidth of 84% is achieved for all scenarios, accompanied by a peak gain of approximately −30.2 dBi. The ultrawideband antenna features two-sectional spiral-shaped radiating patches along with a slotted ground. A coaxial feed is connected to one end of the printed spiral for excitation. The spiral geometry of the patch enhances the antenna's electrical length and −10 dB bandwidth. The simulated maximum gains are documented as follows: −28.6 dBi in the homogeneous skin box, −30.2 dBi in the realistic human heart, −27.7 dBi in the scalp, and −28 dBi in the hand. The measured peak gain is −29.3 dBi in minced pork. For the capsule-type device in the heart, peak SAR values are measured at 796.1 and 64.1 W/kg at a 1 W input power. With varying bit rates and input powers, it demonstrates communication capabilities over distances of 1.2 m, 3 m, 9 m, and 30 m, respectively. At a transmission reach of 11 m and a rate of 70 Mb/s at 25 mW, the system proves suitable for high-data-rate applications, including video streaming during surgeries, capsule endoscopies, etc.

A miniaturized CP antenna for implantable applications operating in the 915 MHz band is presented in [21]. The size reduction is achieved through the incorporation of various slots, effectively extending the current path. A shorting pin is utilized to reduce the resonant frequency and improve the purity of CP. The positioning of the shorting pin and the adjustment of the U-shape slot width play a crucial role in achieving a superior left-handed CP (LHCP). It exhibits a wide AR and an impedance bandwidth. SAR value reaches 778 W/kg. In the simulation outcomes using a single-layer cubic skin phantom, there is an observed impedance bandwidth of 12.2% and a 3dB AR bandwidth of 19.7%. Experimental assessments conducted in a skin-emulating solution reveal a measured bandwidth of 17.5%, with an insertion depth of 4mm into the simulated human skin. It achieves a maximum gain of –32.8 dBi. Reflection coefficients remain stable when the antenna is implanted in skin or muscle, maintaining its CP property at 915 MHz when implanted in muscle. However, the resonant frequency shifts to a higher value when the antenna is implanted in the fat layer, attributed to its lower relative permittivity compared to skin.

A 2.4 GHz ISM-based broadband CP implantable patch design for biomedical devices is presented in [2]. The antenna achieves a small volume of $9.8 \times 1.27\ mm^3$ through the strategic use of slots in the patch and shorting pins. Simulations conducted on a sophisticated skin phantom unveil a remarkable bandwidth of 21.5% for impedance and 15.8% to a 3dB AR. Sensitivity involving diverse body

phantoms is detailed, with experimental trials conducted in skin-emulating gel and ham yielding practical impedance bandwidths of 25.9% and 25.7%. The 1g averaged SAR for a three-layer tissue stands at 524 W/kg, ensuring stringent compliance with IEEE safety standards. Peak gain registers at an impactful −33 dBi, coupled with an appreciable radiation efficiency of 0.027%, and implantation is at a mere 3mm depth in the skin.

For advanced medical implants, particularly in applications such as cardiac pacemakers, the adoption of RF-based wireless power transfer is advantageous. An innovative wideband numerical model (WBNM) tailored for deeply implantable antennas and RF-powered leadless pacing is shown in [22]. The model leverages a wideband tissue-simulating liquid (TSL) and a dielectric probe. WBNM is characterized through a hybrid simulation method, amalgamating the finite-element method and method of the moment based on precisely measured TSL properties. Experimental and analytical validations, employing a reference microstrip antenna, attest to the WBNM's prowess in designing deep implantable antennas across a wide frequency spectrum from 800 to 5800 MHz. The technology of integrating a compact conformal antenna alongside a pacemaker makes it possible to have a wireless pacemaker that is highly beneficial medically safe and feasible, especially for deep implants. Simulations showcase an impressive cumulative gain of 5.8 dB with a substantial 10 dB bandwidth spanning 300 MHz.

Wireless capsule endoscopy (WCE) antenna that operates in the MICS band (401–406 MHz) is presented in [23]. The bandwidth of the presented antenna ranges from 284 to 825 MHz. At 403 MHz, this antenna has a maximum realized gain of –31.5 dBi. To comply with the IEEE standards of SAR, the maximum input power is 1.7 mW. The antenna's tolerance is investigated because of bendability and various WCE shell thicknesses. Besides the miniature color video camera, WCE consists of a casing, transmitter, batteries, image sensor, lens, LEDs, and a transparent dome. The wireless capsule is 11 mm × 26 mm in size and weighs approximately 4g. The dimensions of the presented flexible implantable antenna are 15 mm × 15 mm × 0.79 mm. The simulated maximum 1 g average SAR value for this implantable antenna is 913 W/kg when the antenna input power is presumed to be 1 W. At 403 MHz, the power delivered to the antenna should be less than 1.7 mW to comply with IEEE SAR regulations (1.6 W/kg). For battery lengths of 5 and 10 mm, the resonant frequencies are 410 MHz and 415 MHz, respectively with a bandwidth of more than 500 MHz in both cases. The radiation efficiency is −35.79 dB without the battery, and −36 dB and −36.51 dB with the batteries of lengths of 5 and 10 mm, respectively.

A design utilizing permittivity and conductivity of the human body is presented for health monitoring applications in [24]. This study delves into understanding the functionality of implantable antennas, specifically tailored for intelligent health monitoring devices. A meticulous comparative analysis is conducted between two variations of capsule antennas. The proposed design introduces a novel concept of an inner-layer implantable capsule dipole antenna. Experimental setups entail a torso-shaped phantom filled with a human body-equivalent liquid, constructed using 2 mm thick fiberglass. Positioned within the phantom is an internal capsule antenna, while an external receiving antenna is placed outside at 74 mm. The capsule design is characterized by cuboid dimensions measuring 30 mm × 10 mm in length and width, respectively with the relative permittivity precisely matching that of air. This innovative approach holds promise for advancing the field of implantable antennas in the realm of intelligent health monitoring devices. Two types of antennas are tested within the capsule. In the initial scenario, a dipole antenna, that is electrically small (<0.15 λ), is positioned within the capsule. It is separated from the liquids in the human body and is situated 4 mm from the center axis. In the final case, a half-wavelength dipole antenna is mounted at the surface of the capsule, contacting the liquid within the human body. It is positioned 5 mm from the center axis. The results indicate that the antenna isolated from the human body liquid exhibits low conductivity loss but poor impedance matching in the 200 MHz to 2 GHz frequency range. Despite achieving high received power, the presented system's size renders it unsuitable for implantable applications.

Brain-machine interface (BMI) placement of implantable and external antennas is a crucial factor, and a design is presented in [25]. Specifically, artificial tissue emulating (ATE) materials, crafted in a semi-rigid state, were used to emulate the characteristics of biological tissues, and their permittivity and tanδ were measured. For antennas implanted in the brain to track wireless brain signals, they must be small, light, and biocompatible. The reviewed antenna is constructed on a Taconic RF-35 substrate, featuring dimensions of 10 × 10 × 0.5 mm^3. This antenna exhibits a gain of −25 dBi in the broadside direction, coupled with a −10 dB reflection bandwidth spanning from 2.42 to 2.50 GHz. Both top and bottom insulators, each with a thickness of 0.5 mm, are also meticulously crafted using the Taconic RF-35. The design demonstrates a strong agreement between simulated and measured performance in free space and the head phantom, highlighting its potential for applications in BMI systems.

In [26], the authors introduce a systematic design approach for creating a printed implantable antenna with CP capability. The antenna is integrated into a lossy material, with a focus on its total QF. A thorough analysis of the precise QF values concerning high-loss tissue and embedded depth is conducted, and these findings are then leveraged to formulate the design specifications for an implantable microstrip patch antenna (MPA). MPA is fabricated and tested for acquiring the practical values of bandwidth, AR, and gain. The presented antenna achieved a 10dB S_{11} bandwidth of 37.47% ranging from 1.93 to 2.82 GHz whereas, the 3dB AR bandwidth obtained is 5.32% ranging from 2.38 to 2.51 GHz.

The peak gain of the presented antenna is −15.87 dBi with an implant depth of 4mm under the skin. It showed that the design has a 1g-averaged SAR value of 217 W/kg whereas, for a 10g average, the SAR is 40.6 W/kg.

A design of a printed dipole radiator for implantable devices operating in the MedRadio spectrum, i.e., 401 to 406 MHz, is presented in [27]. A simple skin-implantable dipole antenna model is presented. The presented antenna has a very thin profile with a volume of approximately 18.1 mm^3. Two symmetrical radiating arms are attached to a 50 Ohms feeding port. Each dipole arm is intricately bent in conjunction with a folding scheme that contributes to the antenna's physical length reduction. The presented antenna is not a closed loop, unlike traditional folded dipoles. Instead, an open-ended formation is made to allow for better impedance matching and miniaturization. The radiating structure has a high permittivity and is filled with a similar superstrate layer. The antenna is placed inside a skin-mimicking cubic model. L-shaped reactive loading sections are also etched inside the antenna structure to essentially shrink the size of the antenna. To test the antenna's practical performance, a liquid skin medium is used. The simulated maximum 1-g and 10-g average SAR values are 426.5 and 96.8 W/kg, respectively, when the presented antenna is presumed to deliver 1 W. The fabricated dipole presents a measured 10-dB bandwidth of 26% along with the maximum gain of about −29.4 dB. Omnidirectional far-field radiation pattern is achieved, and an average SAR constraint is met when power is below 3.75 mW.

Another design of a CP patch antenna exhibiting a broad bandwidth for implantation into a human body is shown in [28]. The ground plane of the presented MPA is the metal shell of the pacemaker. The embedded depth of this antenna in one layered skin model is 15mm. The developed MPA achieves a broad bandwidth of 61.5% ranging from 1.62 to 3.06 GHz. The 3-dB AR bandwidth achieved in the cubic human skin model fully covers the 2.4 to 2.48 GHz ISM band. Furthermore, according to the analysis on sensitivity and model viability, the presented antenna shows strong tolerance to a variety of tissues.

A similar design of an MPA is presented in [29]. The MPA is conceptualized as a resonator characterized by an exceptionally low and stable QF. Consequently, achieving a substantial impedance bandwidth becomes feasible within a high-loss environment. The presented MPA is fabricated and tested with an embedded depth of 20mm. The presented antenna is designed to operate in the 2.4 GHz ISM band. The simulated bandwidth of the presented MPA ranges from 2.09 GHz and 4.14 GHz (65.8%) possessing a maximum gain of −17.3 dBi. Also, the maximum averaged SAR in 1-g of human skin at 2.4 GHz is estimated to be 226.5 W/kg if the input power is 1 W. To comply with the IEEE C95.1-1999 requirements, the maximum input power in a one-layered skin model should be less than 9.5 mW.

A design of a multi-resonant loop antenna for on-body applications is presented in [30]. The loop antenna is reshaped from a narrow square to a wide and flat structure for an increased bandwidth. An equivalent circuit is built that models the change in impedance induced by variations in the shape of the loop antenna. The optimized antenna is prototyped and tested for wearable applications. The antenna has a measured radiation efficiency of −5.0 dB at 2 GHz when placed inside a human tissue phantom.

A design of an ingestible encapsulated antenna for med-radio frequency is presented in [31]. To shield the antenna from direct contact with human tissue, the same material is used as the superstrate. This also results in an improvement of the overall bandwidth. The meandered strip is divided into two parts, each with a different width. The narrow part's width is set to 0.3 mm, while the wider part's width, called S, is changed to alter the strip's electrical length. For a better impedance matching, one end of the dipole arm is modified to a spiral shape. The dipole is fed at three separate locations. The choice of the feeding locations directly affects the impedance matching. The presented antenna has a compact size of 329 mm^3. The antenna is simulated in one layered skin model with a depth of 3mm. Measurements are conducted in a skin-simulating gel to validate the wide bandwidth performance. The simulation results for the dipole without the strip show that a bandwidth of 25.7% is achieved ranging from 338 to 438 MHz whereas, that for the dipole with the strip is 37.8% covering 348 to 510 MHz. The radiation efficiency obtained is below 0.02% with a peak gain of −35 dBi at 402 MHz. The maximum value of 1-g averaged SAR is 463 W/kg at 402 MHz. To comply with the IEEE SAR standard C95.1-1999 (1.6 W/kg), the input power must be restricted to 3.5 mW. The presence of the battery has an impact on the performance of the presented dipole antenna since it lacks a ground plane. However, an appropriate bandwidth can still be covered for a battery placed at 0.2 mm spacing. The presented antenna is also assessed with a flexible polyimide material as a substrate with a thickness of 0.15 mm. The substrate is bent to make a cylinder shape and its performance is compared with the planar design. Similarly, the peak gain obtained for cylindrical configuration is −37 dBi at 402 MHz which is 2 dBi lower than that of the planar design. Lastly, the SAR analysis of the presented design shows that the maximum value of 1g averaged SAR is 485 W/kg at 402 MHz which complies with the IEEE SAR standard C95.1-1999 if the input power is restricted to 3.3 mW.

A design of an annulated circular antenna is shown in [32]. This work introduces a CP antenna designed for biomedical applications, specifically operating in the ISM band. The design originates from a basic pin-loaded patch, incorporating CP characteristics. To enhance performance, a dual-mode pin-loaded annular ring is implemented to bring additional resonant frequency. A pair of closely spaced rectangular patches are used to bring closer the resonant frequencies in the case of muscle implants. Furthermore, size miniaturization and improved impedance matching are achieved by adding arc-shaped slots. The volume of the

presented antenna is $\pi \times 25 \times 1.27\ mm^3$ and is implemented with an implant depth of 3mm. The presented design has an 8% simulated impedance bandwidth and a 19.1% broad AR bandwidth. Right hand (RH)-CP is accomplished with a maximum realized gain of −22.7 dBi at boresight. At 2.45 GHz, the maximum simulated 1-g averaged SAR value is 508 W/kg when the input power is set to 1 W. The design is applicable for neural signal recording and the maximum permitted input power is −19 dBm.

A CP antenna system for wireless power transmission is presented in [33]. The antenna uses capacitively coupled stubs to achieve a miniature volume of $11 \times 11 \times 1.27\ mm^3$. An external CP antenna is also developed to establish wireless power transfer. The antenna structure has thicknesses of 0.5 mm and 4 mm, respectively, with an air gap of 20 mm. To achieve CP, the microstrip line between adjacent metal pins is designed with a quarter-wavelength path length. Simulated results demonstrate that the implantable antenna possesses an impedance bandwidth from 889 to 924 MHz whereas, the bandwidth to AR is narrower, spanning over 901 to 912 MHz. The dominant polarization of the antenna is right-handed CP (RHCP), showcasing a notable CP discrimination of 20 dB in the primary radiation direction. The simulated peak realized gain registers at −29 dBi, observed at 910 MHz. The external antenna, simulations reveal an impedance bandwidth ranging from 828 to 982 MHz (17%), accompanied by an AR bandwidth spanning 880 to 930 MHz (5.5%). The external antenna achieves a peak realized gain of 8 dBi at 915 MHz. A rectifier is employed to convert RF power captured by the implantable antenna's aperture into DC power. The power levels of interest range from 20 to 10 dBm, with corresponding conversion efficiencies of 23% and 44% at these power levels. Testing involves embedding the antenna in minced pork and positioning the patch antenna between the external antenna and the pork's edge at 0.4 m. The rectifier circuit yields an output voltage of 0.136 V, resulting in a converted DC power of 5.14 W when the external antenna's maximum input power is 25 dBm. The maximum EIRP reached is 33 dBm.

A low-profile implantable microstrip CP antenna with a volume of 91.9 mm^3 is shown in [34]. The antenna design incorporates crossed slots into a circular patch to achieve CP performance. Due to the lossy tissue environment in which it operates, additional LC (inductive-capacitive) elements are introduced to meet the 50-ohm impedance matching requirement. The antenna's edge is loaded with arc-shaped slots and shorting pins, complementing the crossed slots in the center. Simulated results demonstrate that the antenna possesses a CP bandwidth of 18.3%, making it well-suited for applications in biomedical devices. To accommodate the size constraints of the antenna inside human tissue, a substrate material with high dielectric properties, such as Rogers 3010, is commonly utilized. This material is employed not only as the substrate but also as a superstrate to maintain separation between the radiation patch and the lossy tissue. Simulated results reveal that the AR below 3 dB covers 2.18 GHz to 2.62 GHz. The presented antenna attains a maximum gain of −20.3 dBi in the +z-direction, indicating that the primary power radiation of the antenna is directed toward the upper surface of the human body. The simulation considers a three-layer model comprising 3 mm of skin, 3 mm of fat, and 54 mm of muscle tissue. At the frequency of 2.45 GHz, the maximum 1g and 10g averaged SAR values are calculated to be 649 W/kg and 280 W/kg, respectively, for an input power of 1 W. Adhering to IEEE safety standards, this limits the input power to 2.4 mW. Measured results demonstrate an impedance bandwidth of 16%, spanning over 2.36 to 2.77 GHz, effectively encompassing the entire ISM band.

Three antenna designs are introduced in [35]. The designs are capacitively loaded loop (CLL), complementary split ring loop (CSRL), and interdigital capacitor loop (IDCL). Narrow slits and gaps are incorporated as capacitors in these designs. In vitro measurements are carried out using CSF samples from pigs of different ages within the sub-1-GHz band (0.1–1 GHz) to investigate potential age-related variations in the dielectric properties of CSF. The results demonstrate a consistent pairwise association between samples, with permittivity exceeding 0.77 and conductivity exceeding 0.83. This suggests that dielectric properties and sensing sensitivity remain unaffected by age. The implantable antennas exhibit a relative resonance sensitivity ranging between 6% and 8%, with a resonance frequency shift between 31–40 MHz. This shift corresponds to a 14% increase in CSF permittivity at 400 MHz. Simulation within a realistic human head model, embedding the antennas in CSF at a 14 mm implantation depth and exciting them with a 0.5 W signal, reveals a relative frequency shift of approximately −5%, −6%, and −7% for the IDCL, CLL, and CSRL, respectively, when the highest permittivity is increased by 14%. Furthermore, the resonance frequency results in a frequency shift of 36 MHz for CLL, 31.5 MHz for CSRL, and 40 MHz for IDCL when immersed in a CSF liquid simulant with a 14% increase in dielectric constant and equivalent conductivity.

A design of a multiband conformal antenna for low-power capsule endoscopy is shown in [36]. Bandwidth enhancement, size reduction, and tuning for the desired frequency are done using the slots and the shorting pins. The substrate used for the presented design is ultralam whereas the superstrate and the capsule shell are of the same material, i.e., polylactic acid. The superstrate is used in the flat form of the antenna to prevent mismatching when incorporated into the capsule. The antenna is designed to cover five bands including the MedRadio, ISM, and the midfield bands. The presented design has a footprint of 57 mm^3 when it is flat and 48.98 mm^3 when it is covered. At 402 MHz, the antenna achieves a wide bandwidth of 27.46% in the homogeneous muscle phantom whereas, the bandwidths achieved at 915 MHz and 1200 MHz are 13.2% and 5.42%, respectively. The assessment of specific absorption rates in different implanted positions complies with the IEEE safe standards. The highest value of SAR is achieved in

the small intestine which is 293.7 for 1 gram of tissue when the input power is 1W at the frequency of 402 MHz. When the antenna is wrapped in the capsule, the bandwidth achieved is 38.6%, 19.6%, and 8.1% at 402 MHz, 915 MHz, and 1200 MHz respectively whereas the gain achieved is −30.8 dBi, −19.7 dBi, and −18.7 dBi, respectively. At all resonance frequencies, the average efficiency of the antenna is greater than −40 dB. A 3D printer is used to build a capsule for enclosing batteries and other circuit elements. This capsule is utilized for conducting measurements within a box filled with minced pork. The antenna's conformal design, omnidirectional radiation, and multi-band flexibility are suitable in capsule endoscopy and biotelemetry applications.

Another research work demonstrating a compact printed antenna with a volume of 17.15 mm^3 is shown [37]. The antenna is a spiral form of a radiating patch that has two symmetrical upper and lower sides. An open-ended slot is etched in the ground plane to achieve size miniaturization and bandwidth enhancement. A planar device for head implantation and an encapsulated wireless pacemaker is developed to connect the antenna with the devices. Moreover, the antenna is held with the electronics and a battery within the system. To prevent close interaction with human tissues, all the elements are enclosed in a biocompatible ceramic alumina. The maximum gain achieved by the antenna is −30.5, −22.6, and −18.2 dB at 402, 1600, and 2450 MHz, respectively. The maximum 1g-averaged SAR value achieved at 402 MHz is 588 W/kg. Similarly, at 1600 MHz, the SAR achieved is 441 W/kg whereas, at 2450 MHz it is 305 W/kg. The practical performance is checked by placing the prototype in a saline solution containing minced pork muscles. In addition, data rates of 7 kb/s and 100 kb/s are used to calculate the practical range for biotelemetry applications.

A design of 3D micro-antennas is shown in [38]. In this work, a self-holding technique is utilized to develop a miniaturized micro antenna with the dimensions of 500 × 500 × 500 μm^3. The presented microcube antenna is optimized to function inside biological tissues. A miniaturization technique using the meandered lines is introduced to adjust the electrical length for resonating at a lower frequency. Four different lengths of meandered line each having eight turns are presented. With the increase of the length of the meandered line, the operational frequency of the design reduces, and the resistance impedance of the antenna increases. The simulated bandwidth of the antenna ranges from 4.8 GHz to 8 GHz. The center frequency of the low-pitch antenna is 7.8 GHz whereas, that of the high-pitch antenna is 7.2 GHz.

In [39], a design featuring a 2.4 GHz compact implantable antenna on a brain phantom is introduced. The antenna's geometric configuration showcases a circular shape crafted to operate with a wide bandwidth and achieve a broadside radiation pattern. For antenna integration, the dura layer is strategically employed immediately after the modulation process, as simulated in full-wave simulation software. The design incorporates an offset-fed meandered antenna featuring two slots. Fabrication utilizes a low-loss Taconic RF-35 substrate, known for its biocompatibility. Furthermore, the practical viability of the presented antenna is checked through testing within a seven-layer phantom containing semi-rigid artificial tissue-mimicking materials. The antenna achieves a 10 dB return loss bandwidth of 13.8% in simulations whereas, in measurements, it is 14.9%. The peak gain obtained is −20.75 dBi with an efficiency of 0.24%. The 1g-averaged SAR value obtained is 568.2 W/kg for an input power of 1W whereas, for 10g-average the SAR value is 84.6 W/kg.

A design of an antenna for biomedical functionalities with a CP capability is presented in [40]. The presented antenna is low profile with an overall volume of 54.9 mm^3. In this design, a square ground with a limited clearance is used. Reactive components are used to achieve CP and good impedance matching. To check the antenna's performance, a simulation analysis is carried out on a single-layer tissue model. The presented antenna has a broad AR bandwidth ranging from 2.331 to 2.582 GHz. The antenna exhibits strong robustness to a variety of implant depths and biocompatible coating thicknesses. The measured impedance bandwidth is 621 MHz over a 2.4 to 2.48 GHz ISM band with a peak gain of −21.1 dBi. A link budget calculation is also carried out considering an external CP antenna. With an input power of 1 watt, the 1-g averaged SAR value obtained is 356.4 W/kg at 2.45 GHz.

A design incorporating a circular implantable antenna with its geometry is presented in [41]. The overall footprint of the presented antenna covers a volume of 797.96 mm^3. Open-ended slots in the ground plane and a superstrate are used to realize the dual-band operation. Pork meat and liquid models are considered for measurements and practical validation. The measured bandwidth of the antenna is 38.1% and 17.6% at the MICS and ISM band, respectively. The peak gain achieved is −34.08 dBi and −15.2 dBi at the MICS and ISM band, respectively. With an incident power of 6.625 mW, the 1g-averaged SAR value obtained is 241.5 W/kg.

Another design with a size of 120 mm^3 and its geometry is presented in [42]. The presented antenna is wideband and is developed to conform to the applications of WCE. To reduce the antenna's size and increase its impedance bandwidth, several slots are inscribed on the radiator and the ground plane. To optimize the impedance matching, the capacitance loading technique is used. When the antenna is implanted in the WCE system, the impact of various organs such as the stomach, small intestine, and colon is examined in a one-layer skin phantom model. Tests on a chicken breast slab are also performed for proof of concept. The impedance bandwidth achieved for the presented antenna is 20.5% covering 2.17 GHz to 2.69 GHz. The conductivity values achieved are 2.21 S/m, 3.17 S/m, and 2.04 S/m in the case of stomach, small intestine, and colon, respectively. The loss tangent obtained is 0.26, 0.43, and 0.28 in the

case of stomach, small intestine, and colon, respectively. The peak gain achieved is −26, −38, and −28.75 dBi, respectively. The maximum SAR value for the 1g of tissue is 712.1 W/kg when the input power is 1W at the frequency of 2.45 GHz. This limits the maximum input power to 3.0, 2.4, and 3.3 mW in the case of the stomach, small intestine, and colon, respectively.

A design of a dielectric-loaded microstrip antenna is presented in [43] for in-body applications. The implantable antenna is conformal and is optimized to function in all high-water content tissues. A 900 mm^3 capsule is used to transform the antenna into a bent form for implantable applications. An integral ground is used to protect the radiator from the inner circuitry. The maximum gain achieved at the resonant frequencies of 434, 868, and 1400 MHz is −28, −16, and −16.1 dB is with radiation efficiencies of 0.4%, 2.2%, and 1.2%.

A design of a flexible implantable antenna is presented in [44]. A compact CP, wideband loop antenna is presented to operate in the ISM bands. A reactive impedance substrate (RIS) is used to increase the antenna's impedance bandwidth and boost its AR performance. The antenna's size is reduced by meandering each loop arm, whilst the RIS's surface wave production and the antenna's open-ended design jointly produce CP waves. A single-layer skin model and certain phantom versions are used to assess the antenna's accuracy. The dual-band CP activity of the presented antenna is a crucial aspect, as it occurs even though the human skin is flexed. With the design being in flat state, an impedance bandwidth of 123% is obtained, with a 3 dB AR bandwidth of 15% and 8.7% at 920 MHz and 2.45 GHz, respectively. Finally, the impact of microelectronic components is examined in order to assess the appropriateness of the design for biomedical systems. The measured peak gain of the presented antenna is −29.33 dBi and −21 dBi in the lower and the upper ISM bands respectively. Whereas the radiation efficiency is 2.6% at 920 MHz and 3.8% at 2.45 GHz. The presented design is flexible with cubic dimensions of $10 \times 10 \times 0.6$ mm^3.

A design for body signals monitoring is presented in [45]. The presented design is skin-adhesive and with a 35-mm diameter. The envisaged adhesive repeater is designed with a sleek and inconspicuous profile, tailored for dual-band operation covering both the ultrawideband (UWB) and ISM spectrum. The antenna consists of three layers, each layer contributes to its compactness and output reliability. To evaluate the repeater's in-body link, a low-profile implantable probe is used. A synthesized medical signal is then transmitted between the two antennas. The results show that the antenna performs admirably in terms of impedance matching and time signal preservation with a fidelity greater than 75% which is essential for impulse radio systems. The realized gain of the antenna varies between −6.6 dBi and −13.5 dBi. The signal-to-noise ratio (SNR) value obtained is above −10 dB.

A design operating at 918 MHz for a radio frequency identification (RFID) antenna is presented in [46]. This is encased in thin sheets of biocompatible PET. The design considers embedding in the fat layer under the flesh, with the muscle serving as a lossy ground plane. A T-slot is used in the patch antenna for impedance matching. The presented antenna is tested with different materials including aluminum tape, ELCOAT ink, and inkjet printing. The ELCOAT ink works similarly to aluminum whereas, inkjet printing produces a very thin film that is susceptible to skin depth impacts. With careful tuning of impedance, the antenna is useful for the skin surface.

A design of a quad-band antenna is presented in [47] for deep-body implants. It introduces a full wireless power transform (WPT) that includes a patterned transmitter, a high-efficiency rectifier, and a system-integrated antenna. The size is 6×6 cm^2 and it has a slotted patch at 1470 MHz. The antenna consists of a printed CP which has a segmented cut meandered line along with the slotted ground. Open-end ground slots are used to bring additional resonances and miniaturization. A matching layer with high permittivity is employed between the WPT and the phantom to enhance the power transfer efficiency of the system. At 2-dBm RF input power, a voltage doubler is also calibrated at 1470 MHz with an RF-to-DC conversion efficiency of 90%. The antenna has a volume of 8.43 mm^3. The gain is −34, −29.6, −28.2, and −22.4 at 403, 915, 1470, and 2400 MHz. The SAR value calculated is 0.187 W/kg when 1g tissue is used with an input power of 1W at 1470 MHz. According to the experimental findings, the device transmits 6.7 mW power to millimeter-sized implants placed 5 cm deep in tissues.

Two designs of flexible UWB antennae for neural recording implantable applications are demonstrated in [48]. The antennas are reconfigurable with dual and single polarization capability. The antennas are designed with the intended use in a nonuniform multi-layer head model. The presented antennas have a wide frequency bandwidth spanning over 2 GHz – 11 GHz covering the ISM band and the UWB frequency band. The dimensions of the single polarization antenna are 12mm × 12mm whereas, those for the dual polarization design are 10mm × 9mm. The dual polarization antenna offers a smaller size, smaller sensitivity to angular misalignment, and more fidelity. In the design of the single polarization antenna, a propagator is designed to maximize the surface current intensity. Also, truncating the ground plane of a transmission line into a staircase shape provided an improved return loss. For dual polarization antenna, a spiral structured propagator is used to induce the current equally in the X and Y axes. The average radiated power for the single polarization antenna is 5 mW whereas that for the dual polarization antenna is 5.7 mW. The antennas are tested using animal brains to assess simulation results.

A CMOS-based rectenna for implantable devices is presented in [49]. This presented integrated on-ship rectenna is extremely low profile with an area of 0.43 $mm^{2.}$ The presented antenna is based on a folded slot topology. The

antenna is designed to resonate at 915 MHz. The rectenna is etched on a high-resistivity Si substrate having a low input power demand. The low power requirement and micro-size make this rectenna an appropriate option for low-power implantable applications. The testing of the rectenna is carried out using a loaf of chicken breast. It is observed that the rectenna has a short range below 8cm with a DC output power of 1.2 mW and rectified voltage of 1.1 V.

A design of a low-SAR implantable antenna is presented in [50]. This study introduces a wideband antenna featuring a coupled ground designed to encompass the MedRadio frequency band. The antenna comprises a sigma-shaped monopole radiator and a C-shaped configuration, strategically engineered to excite two modes that effectively regulate the near-field distribution, ensuring low SAR. The overall volume of the presented design is 560 mm^3. For an input power of 1W, the peak value of 1g-averaged SAR is 161 W/kg. The peak realized gain of the design is −27.8 dBi over a wide spectrum of 67.8% (360 MHz – 720 MHz). Measurements have shown that a resonance frequency shift occurs when the bending curvature is changed from 15 mm to 100 mm.

A design for wireless power transfer is presented in [51]. In this work, an implantable rectenna system is presented to operate in the ISM band. To couple the emitted energy coming from the outside patch antenna, a coaxial-fed circular antenna is designed which converts this energy into DC power by using a rectifying circuit. The designed circular antenna consists of a patch wherein two circular slots are cut. A metallic reflector is used to improve the reception. This reflector is placed behind the human body. The reflector improves the S_{21} by 8 dB when the implantation depth is 16 mm at the transmission distance of 400 mm. The efficiency of the rectifying circuit and the whole system is assessed. The rectifying efficiency of the circuit is 59.7% whereas, it is 68.9% when the transmission distance is 200 mm. For the practical validation of the performance of the transmission link, the transmission distance is fixed at 400 mm. The measurements are carried out on both porcine and bovine tissue. The measured gain of the presented antenna is −29.8 dB and −23.2 dB without a reflector and with a reflector, respectively when the implantation depth is 16 mm. For 10 mm depth, the measured values of the gain are −30.9 dB and −26.5 dB, respectively.

Another design of a miniature antenna is presented in [52]. In this work, a miniaturized implantable antenna is presented with the capability of microwave backscattering at the 2.4 GHz and 2.8 GHz frequencies. The presented design is suitable for batteryless implants, especially those which are able to receive power from the outside at 2.4 GHz and able to backscatter it at 4.8 GHz. The presented design contains an E-shaped patch with meandering arms and shorting pins. The overall volume of the antenna is 53.13 mm^3. The meandering arms and the shorting pins reduce the size of the antenna by 39% while also increasing the gain by 10.3 dB and 2.6 dB at 2.4 GHz and 4.8 GHz, respectively. The fabrication of the antenna is done on a high permittivity board. The broadside realized gain obtained is −16.7 dB and −12 dB at 2.4 GHz and 4.8 GHz, respectively. A post-mortem human subject (PMHS) evaluation is used to verify the antenna's accuracy under anatomically correct conditions. Six PMHS locations are tested for the reflection coefficient. It is found that the design exhibits a reflection coefficient of less than −4.5 dB which means that in all the scenarios, at least 64.5% of the supplied energy pours into the antenna.

Two designs of implantable antennas are presented for ISM frequency in [53]. Firstly, a helical antenna is developed in a one-layer muscle phantom. For wireless implanted devices with a fixed implant location, a second implanted patch antenna is constructed in a one-layer skin phantom. The dimension of the helical antenna is $\pi \times (5.5)^2 \times 3.81\ mm^3$ whereas the dimensions of the patch antenna are 10 × 10 × 1.27 mm^3. At the Singapore Institute for Neurotechnology, the two antennas were surgically inserted into the rat. To assess the antennas' sensitivity, the measured results in a rat are compared to the simulated one-layer results. The helical antenna has 3 open loops within a multilayer PCB which are connected through via holes to make an axial helix. The AR bandwidth in the case of a helical antenna ranges from 2 to 2.8 GHz whereas, in the case of a patch antenna it is 2.44 to 2.48 GHz. The center frequency for the helical antenna is 2.1 GHz whereas, for the patch antenna, the resonant frequencies are 2.18 and 2.3 GHz. The in-vitro measurements resulted in reduced impedance bandwidths as compared to the simulated results. Moreover, significant frequency shifts are observed. The frequency shift for the helical antenna is −12.5% whereas, for the patch antenna the frequency shifts are −11% and −6.1%.

In [54], a wideband antenna is presented for wireless capsule endoscopy systems. The main capsule has a size of 11 mm × 22 mm, and it consists of an integrated antenna design and electronic components. The copper cylinder also minimizes EM interference from batteries and electronic circuit components. When antenna is placed in tissue, it provides a wide bandwidth which ranges from 0.721 GHz to 1.705 GHz covering both the ISM and wireless medical telemetry service bands. A stable omnidirectional radiation pattern is achieved when the antenna is placed inside the human tissue. Two sizes of tissue are used to check the radiation performance of the presented system. Considering the tissue size of 110 mm × 80 mm the maximum gain achieved is −13 dBi and −16 dBi at 0.915 GHz and 1.4 GHz, respectively. The radiation efficiency obtained is 2.97% and 1.69% respectively. When the tissue size is 220 mm × 160 mm, the maximum gain achieved is −28.2 dBi at 0.915 GHz and −29.4 dBi at 1.4 GHz, whereas the radiation efficiency is 0.11% and 0.04%, respectively. When an input power of −25 dBm is supplied, the calculated SAR value is 290 W/kg. To minimize the effects of cables the external antenna used is a bottom-fed patch antenna with a gain of −0.2 dBi and 1.7 dBi at 0.915 GHz and 1.4 GHz,

respectively. The distance between the two antennas varied from 200 mm to 600 mm. It has been observed from the results that as the distance increases, the coupling strength reduces. Moreover, the coupling strength is lower at 1.4 GHz because of greater absorption by the tissues. The bandwidth achieved in the measurements is 984 MHz which is approximately 81%.

Another design of a miniaturized CPW-fed implantable antenna is presented in [55]. This work introduces a monopole patch antenna featuring three split ring resonators and a rectangular slot, coupled with CPWG feeding as a radiating element. The antenna's dimensions are 24 × 22 × 0.07 mm^3. Simulations and testing in both free space and in vitro conditions are employed to assess the effectiveness of the antenna. In free space, the measured bandwidth of the antenna spans over 2.14 GHz to 3.32 GHz, achieving a peak gain value of 2.62 dB. For in-vitro testing, a muscle-mimicking phantom gel is used, and the measured bandwidth of the antenna is 2.15 GHz to 2.75 GHz, with a peak gain of −34.68 dB. Additionally, SAR values are calculated for each scenario. The results indicate that the SAR values fall within the guidelines set by the Federal Communication Commission (FCC), with a maximum SAR value of 0.914 W/kg.

A high-gain, metamaterial-loaded, CP antenna designed for implantable applications is presented in reference [56]. This antenna is versatile and intended for various biomedical applications, operating in the dual bands of ISM 902 MHz to 928 MHz and ISM 2400 MHz to 2480 MHz. Key features of the presented antenna include a ground plane, a substrate, a serpentine-shaped radiating patch, a superstrate, and a metamaterial (MTM) surface. The antenna is fed from the bottom using coaxial feed and shorting pins. The superstrate, characterized by a high dielectric constant, plays a role in stabilizing and decoupling the antenna. Integration of the MTM structure with the superstrate enhances the peak gain, achieving −17.1 dBi in the lower ISM band and −9.81 dBi in the upper ISM band. The backscatter radiation is reduced with the help of a slot-free ground plane of the antenna. For experimental validation, a 3D housing is developed to enclose the antenna, batteries, and the related electronics. The evaluation is carried out in minced pork muscle. The measured impedance bandwidth in the lower and upper bands is 35.8% and 17.8%, respectively. SAR values, calculated for 1 g of tissue, are 576.1 W/kg in the lower ISM band and 524.3 W/kg in the upper ISM band. For 10 g of tissue, the SAR values are 54.5 W/kg in the lower band and 50.2 W/kg in the upper ISM band. The computed data rates for wireless communication are 100 Kbps at 915 MHz and 1 Mbps at 2.45 GHz.

Another design of a miniaturized CP Loop antenna is shown in [57]. The presented antenna consists of four small patches which are attached to the loop along with four high impedance lines individually at four quadrants. Moreover, there are two shorting pins located in the 1^{st} and 3^{rd} quadrants whereas the feed point is located in the 4^{th} quadrant. It has been noticed that there is symmetry in all the loadings across the original point. In this antenna configuration, a RHCP is achieved. To get a LHCP the positioning of the shorting pins and the feeding point can be adjusted. The antenna is designed for implantable applications operating in the ISM 902 MHz to 928 MHz frequency band. Four LC loadings are embraced to establish a slow wave effect to reduce the size of the presented antenna. This resulted in a reduction of the antenna size by approximately 54.4%. The total volume of the design is 214.62 mm^3. The gain achieved is −32 dBi at 915 MHz in simulations. For measurements, skin-simulating gel and ham meat are used. The tested bandwidth achieved is 27.8% for skin and 29.4% for ham meat. The 1g-averaged SAR value evaluated for an input power of 1W is 599 W/kg. This limits the maximum input power to 2.6 mW.

In [58], a two-antenna system is presented for skin implantation. The antennas have overall volumes of 617 mm^3 and 510 mm^3. The antennas are designed to operate in multiple bands including MICS and ISM bands. The configuration of the switching algorithm for efficient system functioning was based on a link budget evaluation. The presented system consists of a planar inverted-F antenna, storage batteries, regulating electronics, and biosensors. The dimension of the antenna is 52.5 mm^3, an antenna has a radiating patch with the shape of serpentine along with the shorting pin, coaxial feed, and ground plane which has a hook-shaped slot that has one end opened to achieve miniaturization. The measurements are taken inside a skin-mimicking semi-solid homogenous phantom to assess the system's performance at 405, 915, and 2450 MHz. For the measurement done on the human scalp, a peak gain of −40.85, −32.98, and −22.37 dBi's is achieved. Similarly, the bandwidths achieved are 64, 91, and 105 MHz, respectively. An analysis of SAR is also shown using 1g of tissue with an input power of 1W. The SAR values computed are 665.35, 837.69, and 759.72 W/kgs, respectively.

A multi-polarization antenna is presented for body-centric biomedical applications in [59]. The design is composed of four dipole radiators to provide switchable linear polarization at 0°, +45°, −45°, and 90°. To induce broadside radiation, a metallic reflector is put beneath the dipoles. To control the selection of a specific dipole, eight pin-diode RF switches are used between the excitation source and the four dipoles. An impedance bandwidth of 34% is attached ranging from 2.2 GHz to 3.1 GHz. The presented system manifests a stable cardioid-shaped radiation pattern throughout the bandwidth with a peak gain of 5.2 dBi. Link analysis shows that the antenna is efficient enough to prevent polarization mismatching polarization and retain a good transmission link.

A design of an ε-shaped antenna is presented in [60]. In this research work, a small implantable design scaling about 11 mm × 11 mm × 1.28 mm is presented for biotelemetry applications in WMTS (1.39 GHz – 1.42 GHz) and ISM (2.40 – 2.48 GHz) bands. The size miniaturization

is achieved by using meandered microstrip lines with variable widths and a printed spiral. A via pin is incorporated to further reduce the size of the presented design. The antenna is fed using a coaxial feed. Throughout the design, simulation, and optimization processes, a skin phantom model is employed to ensure realistic performance and behavior in the intended application. The measured bandwidth achieved for the WMTS band is 1.395 GHz – 1.44 GHz whereas that for the ISM band is 2.39 GHz – 2.45 GHz. It is also observed that the radiation pattern for both bands is unidirectional with an achieved gain of −22.06 dB for WMTS and −21.66 dB for the ISM band. For SAR analysis, the antenna is placed in a skin with a depth of 3mm and an applied power of 10 mW for both bands. The 10g-averaged value of SAR achieved is 1.5977 × 10-2 W/kg for WMTS and 1.4977 W/kg for the ISM band. Lastly, the radiation efficiency achieved for the WMTS band is 0.6145% whereas, for the ISM band it is 0.93%.

A polarization reconfigurable Planar Inverted-F Antenna is presented in [61]. The antenna is modeled to function at 2.45 GHz. To overcome the mismatch in polarization and multi-path reflection in an indoor environment, the reconfigurability of two polarizations is done in the antenna. Pin diode switches are used along x and y directions to switch between two orthogonal linear polarizations. The performance of the presented antenna is checked in different complex environments such as muscle layer phantom, multi-layer phantom, and 3D human model. Moreover, in-vitro testing is conducted to verify the presented design. To avoid the undesired impact of the lengthy cables, a sleeve balun is fabricated and inserted into a semirigid coaxial cable. The measured impedance bandwidth achieved is 9.1% ranging from 2.3 to 2.52 GHz. The peak gain achieved in the muscle layer is −24.5 dBi.

Another design of a reconfigurable antenna is presented in [62]. The presented antenna is a radiation pattern reconfigurable antenna with an overall volume of 193.2 mm^3. The antenna is designed to operate in the MedRadio band with a frequency range of 401 to 406 MHz. The size miniaturization is done by spiraling a monopole. For simulations and in-vitro testing, a one-layered skin model is used. The antenna's top and bottom layers are connected using a shorting pin. A microstrip feeding is etched at the top side of the board whereas the bottom side consists of the ground plane and the spiral portion of the antenna. The presented antenna gives three different states of the radiation pattern. The selection between the states is achieved by using two switches which are placed near the shorting pin. The switching between the states does not majorly change the resonant frequency. The maximum frequency shift observed due to switching is 4 MHz. The simulated gains achieved at 403.5 MHz are −19.99, −20.08, and −20.03 dBs in the three states of the radiation pattern. The 1g-averaged SAR values computed for 1W of power are 162.47, 113.36, and 113.92 W/kg, respectively.

A design of a RHCP antenna is presented in [63]. The presented antenna consists of a patch with walls across. Pin loading is used for getting two non-degenerative orthogonal modes. Two open-ended slots were carved on the patch to bring the two modes' resonance frequencies closer together while establishing a 90^0-phase difference. The walls are used to shield the antenna from the lossy tissues to minimize the gain loss. The presented antenna is fabricated on Rogers 3010 board which has high dielectric properties. As a result, the size of the antenna was reduced to 17 mm × 9.6 mm. The top layer of the presented design is a dotted path whereas, the bottom layer is a plane ground with two vias. A superstrate layer is also used for preventing contact with a human body which can shorten the antenna. Moreover, a coaxial feed is used from the bottom side for the ease of implantation. According to the simulations, the impedance bandwidth achieved is 23.1% along with an AR bandwidth of 12.8%. The walls improved the gain of the antenna by 1.5 dBi resulting in a gain value of −21.6 dBi. For measurements, minced pork and skin-mimicking gel are used. When 1W of power is fed to the antenna, the 1g-averaged SAR value obtained is 445.7 W/kg at 2.45 GHz. The maximum allowable input power is 3.59 mW to comply with the safety standards of IEEE [64], [65].

III. SUMMARY OF LITERATURE REVIEW

This review encompasses more than 60 papers sourced from reputable journals. The analysis reveals that a considerable number of the designs featured exhibit low gain, making them unsuitable for portable devices. The effectiveness of detection and monitoring is compromised when employing antennas with low gain, particularly in scenarios with high input power, leading to inherent limitations. Direct contact with body tissues has been observed to significantly diminish antenna performance. Hence, it is a critical need to develop on-body and implantable antennas that can operate on battery power while demonstrating commendable gain and efficiency. Table 1 provides a concise summary of the reviewed designs.

IV. COMPARISON AND ANALYSIS

A. ANTENNA GAIN

A comparison of the gains between the reviewed designs is presented in Figure 1. It is observed from the figure that most of the designs possess poor gain due to the presence of skin, muscle, and tissue layers. Very few designs have gain values greater than 0 dB. The design presented in [4] has a gain of 0.8 dB which was calculated without considering skin layers, thus it was not realizable for implantable applications. The design presented in [19] has a gain of 0.64 dB obtained from in–vivo measurements. The gain of the antenna presented in [22] is 5.8 dB and was not considered for the implantable scenario. The gain of this antenna would be lower when measured with skin, muscle, and tissue layers. Lastly, the design presented in [59] is not for implantable applications and thus its gain was considered as an outlier.

TABLE 1. List of designs and key parameters.

S/N	Antenna Type	Frequency Band (GHz)	Dimensions (mm^3)	Gain (dBi)	Radiation Efficiency (%)
1	CSRR	0.403, 2.45	-	-26, -15	0.12 @ 0.403, 0.53 @ 2.45
2	Patch	2.35-2.50	90 × 90 × 25.27	-27.2	5.45- gel, 5.69- pork
3	Coaxial dipole	85, 179, 275 MHz	85 cm	-	-
4	WLAN	2.4, 5.8	Flexible	-5.4, -3.8	-
5	CPWG	ISM band	10 × 10 × 0.4	-12	2.5-5.6
6	HF/UHF	902-928 MHz	-	17% - HF 38 dB- UHF	-
7	Rectenna	915, 2.45	16 × 14 × 1.27	-24.3	5.7
8	Transceiver	MICS band	2 mm^2	-	90 dBm sensitivity
9	Med Radio	403	12.5 ×12.5 ×1.27	-32.49	6.15- simulated
10	Annular-ring	2.31-2.51	120.69	-	2.49-3dB AR
11	CP	2.32-2.62	-	-17	13-pork
12	Biotelemetry	915, 2450	434.72 mm^3	-28.04	-
13	MIMO	2.14-2.58	18.5 × 18.5 × 1.27	-15.18	18.64
14	Multiband	915, 2.45	7 × 7.2 × 0.2	-28.44	-
15	Triple band	ISM, midfield	647(capsule), 425.6 (flat)	-26.4, -23, -20.47	-
16	Rectenna	673 MHz	5 × 5 × 3.2	-15.37	40
17	Biosensor	0.5, 2.45	16	-	-
18	Biotelemetry	389-419 MHz, 2.39-2.56 GHz	-	832, 690 W/kg	-
19	Pacemaker	924	-	0.64	-
20	UWB	-	28.85	-30.2	-
21	CSRR	2.4, 5.8	15 x 10 x 1.5	2.5	60
22	Patch	2.4	20 x 8 x 1.0	1.8	55
23	Coaxial dipole	5.8	18 x 12 x 2.0	3.2	70
24	WLAN	2.4	22 x 10 x 1.5	2.0	65
25	CPWG	2.4	25 x 15 x 1.8	2.1	63
26	HF/UHF	5.8	12 x 8 x 1.2	1.5	50
27	CSRR	2.4, 5.8	20 x 12 x 1.5	2.3	58
28	Patch	2.4	18 x 10 x 1.0	1.9	54
29	Coaxial dipole	2.4	15 x 8 x 1.0	1.6	52
30	WLAN	5.8	20 x 10 x 1.8	3.0	72
31	CPWG	2.4	25 x 15 x 1.5	2.2	60
32	HF/UHF	5.8	10 x 5 x 1.0	1.8	55
33	CSRR	2.4	22 x 12 x 1.2	2.5	65
34	Patch	5.8	18 x 10 x 1.5	2.9	68
35	Coaxial dipole	2.4	15 x 7 x 1.0	1.7	53
36	WLAN	5.8	20 x 12 x 1.5	3.1	70
37	CPWG	2.4	18 x 10 x 1.0	2.0	60
38	HF/UHF	2.4	22 x 12 x 1.5	2.3	62
39	CSRR	5.8	10 x 5 x 1.0	1.6	50
40	Patch	2.4	20 x 12 x 1.2	2.1	58
41	Patch	2.33-2.58	54.9	-21.1	35.64
42	Circular	MICS, ISM	797.96	-34.08	38.1, 17.6
43	Wideband	2.17 - 2.69	120	-26	20.5
44	Dielectric-micro-strip	0.434, 0.868, 1.4	900	-28	0.4 - 2.2
45	Flexible CP loop	0.92, 2.45	10 x 10 x 0.6	-29.33, -21	123
46	Skin-adhesive	UWB, ISM	35 (diameter)	> -13.5	75
47	Subdermal RFID	0.918	Thin sheets	N/A	Tunable impedance
48	Quad-band	0.403, 0.915, 1.47, 2.4	60 x 60	-34, -29.6, -28.2, -22.4	N/A
49	Flexible UWB	2 - 11	12 x 12, 10 x 9	5, 5.7	N/A
50	CMOS	0.915	0.43	N/A	1.1 V
51	Wideband	0.36 - 0.72	560	-27.8	Wide AR bandwidth
52	Implantable rectenna	0.902-0.928, 2.4-2.48	Coaxial-fed	-29.8	59.7 rectifying efficiency
53	Miniaturized	2.4, 4.8	53.13	10.3, 2.6	N/A
54	Helical and patch	2 - 2.8, 2.44 - 2.48	$\pi \times (5.5)^2 \times 3.81$, 10 x 10 x 1.27	N/A	N/A
55	Wideband	0.721 - 1.705	11 x 22	-13	81
56	CPWG	2.14 - 3.32	24 x 22 x 0.07	2.62	SAR within FCC
57	Metamaterial-loaded CP	0.902-0.928, 2.4-2.48	High dielectric constant	-17.1, -9.81	35.8, 17.8
58	CP loop	0.902	214.62	-32	27.8, 29.4
59	Dual	0.405, 0.915, 2.45	52.5	-40.85, -32.98, -22.37	Miniaturization
60	Multi-polarization	2.2 - 3.1	N/A	5.2	N/A
61[1]	Patch	5.8	7.7 x 6	1.2	51

B. ANTENNA EFFICIENCY

An efficiency comparison between the reviewed designs is presented in Figure 2. It can be observed that for most of the designs, the efficiency value is closer to or less than 5%. The graph has two outliers for [6] and [30]. Both measurements were taken for external applications making the efficiency

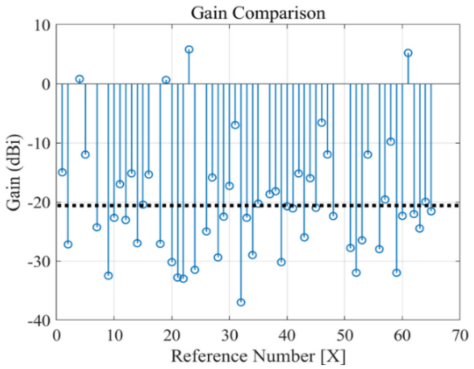

FIGURE 1. Gain comparison between the reviewed antennas.

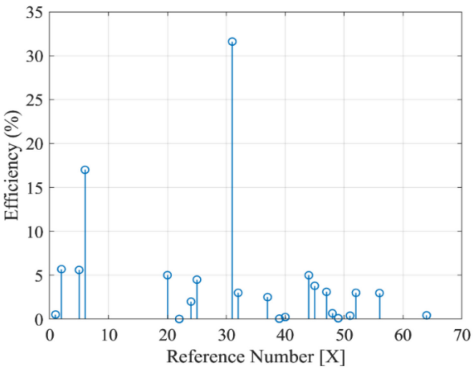

FIGURE 2. Efficiency comparison of the reviewed antennas.

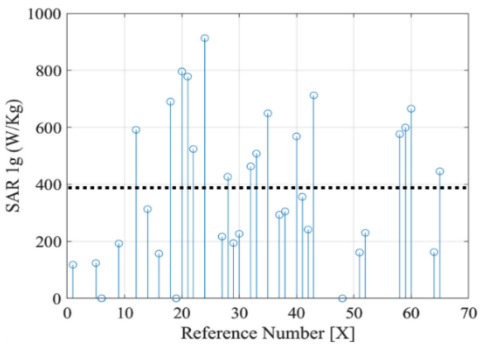

FIGURE 3. SAR comparison between the reviewed antennas.

values higher than the implantable antennas. Due to the presence of skin, muscle, and tissue layers, the reactive near field and radiative near field of an antenna suffer a huge power loss that gets absorbed or dissipated resulting in poor on–body or implantable performance.

C. SPECIFIC ABSORPTION RATE (SAR)

A line graph presenting the SAR values for the reviewed antennas is shown in Figure 3. The SAR values are 1g–averaged. The majority of the designs presented in this paper have acceptable SAR values. The designs for which SAR value is higher, the input power is reduced to meet the practical standard. This means that the input power is not a fixed value for all designs and is varied according to the

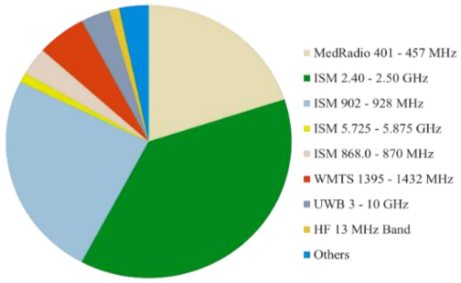

FIGURE 4. Design frequencies for the reviewed antennas.

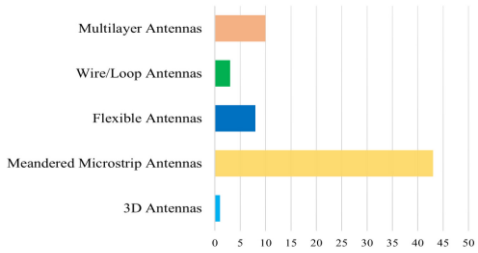

FIGURE 5. Types of Antennas considered for applications.

practical requirements. The FCC set limit for SAR is 1.6 W/kg when averaged over 1g of actual tissue whereas, for 10g of actual tissue, the acceptable limit of SAR is 2.0 W/kg. The SAR value among the reviewed designs is maximum in [23]. The SAR value is 913 W/kg which suggests that the given power cannot be more than 1.75 mW at which the SAR will meet the standard threshold of 1.6 W/kg [64], [65].

D. FREQUENCY OF OPERATION

An overview of various frequencies over which the reviewed antennas are designed is shown in Figure 4.

It can be observed from the figure that the antennas reviewed are designed majorly for ISM bands. The largest proportion of the designed antennas is for ISM 2.40 – 2.50 GHz frequency band whereas, the second largest is for ISM 902 – 928 MHz. Almost all the designs are modeled for less than 6 GHz.

E. ANTENNA TYPES

An overview of the types of antennas of which this review is carried out is shown in Figure 5.

The figure presents different shapes of the antennas that are presented in the literature for the design of on–body, implantable, and other medical antennas. It can be observed that the majority of the designs considered in this review are microstrip-based with meandered configurations for small volumes. There is a small proportion of flexible and multilayer antennas whereas 3D antennas are rare. The flexible antennas are usually better for on-body and wearable applications whereas, meandered microstrip antennas provide a better radiation performance while covering lower frequency bands within a small volume. 3D designs can be an interesting point of research to consider for medical

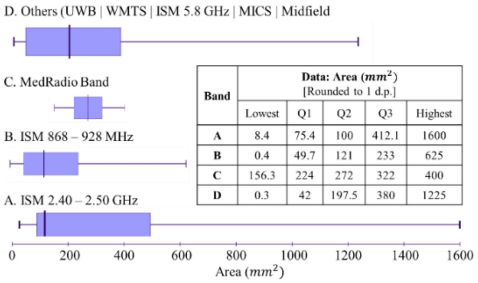

Band	Data: Area (mm^2) [Rounded to 1 d.p.]				
	Lowest	Q1	Q2	Q3	Highest
A	8.4	75.4	100	412.1	1600
B	0.4	49.7	121	233	625
C	156.3	224	272	322	400
D	0.3	42	197.5	380	1225

FIGURE 6. Size analysis of the reviewed antennas.

applications possibly to overcome the gain and efficiency losses due to the skin layers.

F. SIZE COMPARISON

An analysis of the dimensions of the antennas is depicted in Figure 6. Box and Whisker plots have been employed to effectively illustrate the broad spectrum of sizes observed across different operational frequencies. The data highlights significant variability in the antenna sizes within the ISM spectrum, ranging from as small as 0.4 mm^2 to as large as 1600 mm^2. This variability underscores the versatility of the ISM band, accommodating a wide array of medical applications that involve devices of varying sizes. In contrast, the antennas within the MedRadio spectrum exhibit a more constrained range of sizes when compared to their ISM counterparts.

G. SUMMARY

Upon analyzing various parameters such as gain, efficiency, SAR, frequency, and antenna types, it can be deduced that the antennas for implantable applications have certain limitations. These constraints such as small size, presence of skin, muscle, and tissue layers, and SAR plays an important role. The implantable and on-body antennas discussed have low gain and efficiency. However, it is a challenging task to adhere to the practical constraints when improving the performance of an antenna. The input power can be increased to improve gain and efficiency, however, exceeding beyond a certain limit will result in a large SAR value, making EM waves harmful to the skin. Non-ionizing radiation is suitable for medical antennas as the ionizing radiation may cause severe skin problems. Despite these challenges, antennas demonstrate a significant potential in providing a wireless sensing and monitoring service. The designs reviewed are mostly at lower ISM and WMTS frequencies. Future research can include higher frequencies especially in millimeter and sub–millimeter range for designing and testing of antennas for medical applications. Moreover, research on the skin, tissue, and muscle layers can be carried out to use their dielectric properties for the enhancement of radiation performance. This has the potential to give rise to a new category of dielectric resonator antennas specifically designed for medical applications.

V. KEY DESIGN CONSIDERATIONS

Designing effective antennas for biomedical applications presents unique challenges due to the complex EM interaction with biological tissues, that absorb and attenuate RF signals. Achieving optimal antenna performance characterized by high gain and efficient operation near the body is paramount for reliable and accurate sensing capabilities. Researchers continue to explore novel antenna designs tailored for both in- and on-body applications, striving to overcome these technical hurdles and advance healthcare technologies. Through a comparative analysis, critical parameters such as gain, efficiency, SAR, antenna type, and operating frequency are evaluated, highlighting current trends and identifying areas for improvement in antenna design for medical applications. This review culminates in the proposal of a new antenna design optimized for the demanding requirements of healthcare environments, aiming to set new benchmarks in performance and compactness. Several design considerations should be considered when designing antennas for medical applications and are discussed below:

A. ANTENNA SELECTION FOR BIOMEDICAL APPLICATIONS

Selecting the appropriate antenna type depends on several key factors, including frequency requirements, size constraints, and performance metrics such as gain, efficiency, and SAR. From the analysis of over 60 recent journal papers, several trends and recommendations emerge such as on-body and implantable antennas.

B. IMPLANTABLE VS. ON-BODY ANTENNAS

For implantable devices, antennas must be compact, biocompatible, and capable of maintaining stable performance despite proximity to biological tissues. On-body antennas prioritize comfort, durability, and reliable data transmission in dynamic environments. Table 2 presents a summary of key wearable antenna designs considered in this review whereas, that for main Implantable antennas is shown in Table 3.

C. FREQUENCY BAND

Antennas operating in the ISM bands are commonly used due to regulatory compliance and compatibility with existing wireless standards in healthcare. Table 4 presents different frequency bands which can be considered for medical applications. These frequency bands are chosen based on their suitability for implantable medical devices and other healthcare applications. The ranges provided cover both licensed and unlicensed bands used globally for various wireless communication purposes in medical contexts.

D. ANTENNA TYPES

Diverse antenna types including patch antennas, spiral antennas, and dipole antennas have been explored for biomedical applications. Each type offers distinct advantages in terms of radiation pattern, bandwidth, and ease of integration so far patch antenna is best.

TABLE 2. Reviewed wearable antennas.

S/N	Antenna Type	Frequency Band (GHz)	Dimensions (mm^3)	Gain (dBi)	Radiation Efficiency (%)
2	CP Patch	ISM (2.35-2.50)	90 × 90 × 25.27	-27.2	5.45% (gel), 5.69% (pork)
14	Multiband	ISM, Midfield	647, 425.6	-	14.7% to 24.8%
20	Tri-band	Biotelemetry	-	-	-
38	Conformal	0.4-2.2	50 x 35	-15	14
45	Flexible CP Loop	920 MHz, 2.45 GHz	10 x 10 x 0.6	N/A	-29.33 dBi, -21 dBi
46	Skin-adhesive	UWB, ISM bands	35 mm diameter	> -13.5 dBi	N/A
55	Wideband	Wireless Capsule Endoscopy	0.721 - 1.705 GHz	Copper cylinder	-13 dBi
59	Dual System	Skin Implantation	405, 915, 2450 MHz	-	665.35, 837.69, 759.72 W/kg

TABLE 3. Reviewed implantable antennas.

S/N	Antenna Type	Frequency Band (GHz)	Dimensions (mm^3)	Gain (dBi)	Radiation Efficiency (%)
1	CSRR	ISM (0.403, 2.45)	0.7	-26 to -15 at	0.12% to 0.53%
3	Coaxial Dipole	85, 179, 275 MHz	85 cm long	-	-
12	ISM Bands	ISM (915, 2450)	434.72	-28.94 -23.06	-
42	Circular	MICS, ISM bands	797.96		-
52	Rectenna	ISM (902-928, 2400-2480)	Coaxial-fed, circular slots	-29.8 dB	-
56	Metamaterial-loaded CP	902-928, 2400-2480	High dielectric constant, MTM surface	-	61%
61	ε-shaped	Biotelemetry, WMTS, ISM bands	1.39 - 1.42 GHz, 2.40 - 2.48 GHz	-	59%
63	Radiation Pattern Reconfigurable	MedRadio band	401 - 406 MHz	-	62%

E. PERFORMANCE METRICS

High gain and efficient radiation characteristics are critical for antennas deployed in biomedical applications to ensure reliable data transmission and minimize interference with physiological signals.

F. SUBSTRATE SELECTION CONSIDERATIONS

The choice of substrate material impacts the performance and effectiveness of antennas in medical settings. The key considerations include:

TABLE 4. Frequency band selection.

Bands	Frequency Range	Typical Applications
ISM Band	2.4 - 2.4835 GHz	Wireless medical devices, body area networks
ISM Band	5.725 - 5.875 GHz	Medical telemetry, wireless sensors
UWB	3.1 - 10.6 GHz	High data rate communication, imaging
GSM	900 MHz, 1800 MHz	Cellular communication
LTE	698 - 960 MHz, 1710 - 2700 MHz	Long-term evolution, wireless communication
WiMAX	2.5 - 5.9 GHz	Broadband wireless access
Bluetooth	2.4 - 2.4835 GHz	Short-range communication
Zigbee	868 MHz, 915 MHz, 2.4 GHz	Low-power, low-data-rate wireless communication
RFID	13.56 MHz, 860 - 960 MHz	Identification, tracking
Medical Telemetry	400 - 406 MHz, 450 - 470 MHz	Medical devices, remote monitoring

- *Biocompatibility:* Substrates must be biocompatible to minimize tissue reaction and ensure long-term implant stability. Materials such as biocompatible polymers (e.g., Parylene-C, Polyimide) and ceramics are preferred for implantable antennas.

- *Dielectric Properties:* The dielectric constant and loss tangent of substrates affect antenna efficiency and bandwidth. Low-loss materials with stable dielectric properties over a wide frequency range are ideal for achieving optimal antenna performance.

- *Mechanical Durability:* Substrates exhibit mechanical robustness to withstand implantation procedures and physiological stresses without compromising antenna performance or patient comfort.

- *Conductive Materials:* Materials such as copper, silver, and gold are used for their conductivity and biocompatibility.

- *Substrate Materials:* As mentioned, biocompatible materials are preferred for their stability and minimal tissue reaction. Advanced materials such as Rogers are being explored for their electrical properties and miniaturization.

Table 5 presents different materials that are used in designing antennas for medical applications.

G. HUMAN BODY MODELS

Accurate human body models are essential for simulating the interaction of antennas with biological tissues. These models help in predicting SAR, gain, and efficiency.

H. PARAMETER OPTIMIZATION

Simulations are used to optimize various parameters, including antenna geometry, material properties, and placement, to achieve the best possible performance.

I. POWER LIMITATIONS

Table 6 presents power limitations for various designs.

Power limitations are crucial considerations for designing implantable antennas to comply with regulatory standards

TABLE 5. Materials for selection.

Material	Dielectric Constant (ε_r)	Tangent Loss (tan δ)
Titanium	5.0 - 15.0	0.001 - 0.1
Platinum	5.0 - 7.0	0.001 - 0.02
Gold	5.0 - 7.0	0.001 - 0.02
Stainless Steel	2.2 - 3.5	0.001 - 0.01
Polymethyl Methacrylate (PMMA)	2.9 - 3.4	0.002 - 0.005
Polyethylene	2.3 - 2.4	0.0002 - 0.0005
Polypropylene	2.2 - 2.3	0.0002 - 0.0005
Polyetheretherketone (PEEK)	3.3 - 3.6	0.004 - 0.01
Polytetrafluoroethylene (PTFE)	2.0 - 2.1	0.0002 - 0.0003
Silicone Rubber	2.9 - 3.3	0.002 - 0.01
Ceramic (Alumina)	9.0 - 10.0	0.0005 - 0.002
Glass	4.5 - 7.0	0.01 - 0.04
Hydroxyapatite	5.0 - 10.0	0.005 - 0.02
Zinc Oxide	8.0 - 10.0	0.01 - 0.1
Magnesium	2.1 - 3.0	0.002 - 0.01
Calcium Phosphate	3.0 - 5.0	0.005 - 0.02
Poly-Lactic Acid (PLA)	3.0 - 4.0	0.002 - 0.01
Poly-Glycolic Acid (PGA)	3.0 - 4.0	0.002 - 0.01
Polycarbonate	2.8 - 3.0	0.002 - 0.004
Carbon Fiber	1.5 - 2.5	0.02 - 0.05
Hydrogel	50.0 - 80.0	0.05 - 0.2
Polyurethane	3.0 - 3.5	0.002 - 0.01
Cellulose	3.0 - 4.0	0.002 - 0.01
Graphene	3.0 - 10.0	0.01 - 0.1
Silver	5.0 - 6.0	0.003 - 0.01
Nickel	8.0 - 10.0	0.02 - 0.05
Lead	7.0 - 10.0	0.02 - 0.1
Tin	3.0 - 4.0	0.02 - 0.1
Indium Tin Oxide (ITO)	10.0 - 15.0	0.01 - 0.1

TABLE 6. Power limitations.

Frequency Band	Power Limitations	Typical Applications
ISM Band (2.4 GHz)	Typically limited to 1 W	Wireless medical devices, body area networks
ISM Band (5.8 GHz)	Typically limited to 1 W	Medical telemetry, wireless sensors
UWB (3.1 - 10.6 GHz)	Power spectral density limits	High data rate communication, imaging
GSM (900 MHz)	Varies by country regulations	Cellular communication
GSM (1800 MHz)	Varies by country regulations	Cellular communication
LTE (698 - 2700 MHz)	Varies by LTE category (e.g., CAT-1 to CAT-20)	Long-term evolution, wireless communication
WiMAX (2.5 - 5.9 GHz)	Typically limited to 4 W	Broadband wireless access
Bluetooth (2.4 GHz)	Typically limited to 1 W	Short-range communication
Zigbee (2.4 GHz)	Typically limited to 1 W	Low-power, low-data-rate wireless communication
RFID (860 - 960 MHz)	Typically less than 1 W	Identification, tracking
Medical Telemetry (400 - 470 MHz)	Varies, often low power	Medical devices, remote monitoring

and ensure safe operation within the human body or in proximity to it. Regulations may vary by region and application, so specific guidelines should always be consulted during design and deployment.

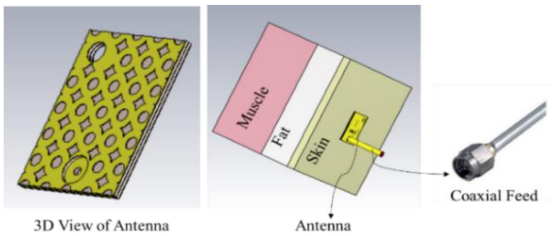

FIGURE 7. Geometry of the antenna for medical applications.

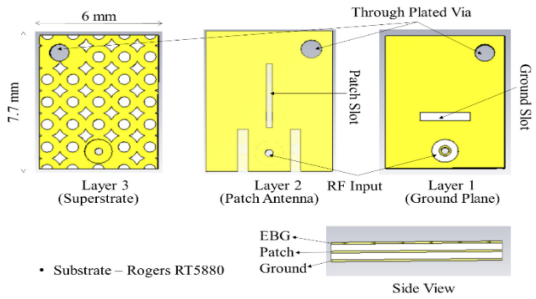

FIGURE 8. Layer–wise geometry of the proposed antenna.

J. CONTACT WITH BODY

Contact with human body tissues is a crucial factor in designing medical antennas. Research has shown that antennas designed with a gap from body tissues exhibit superior performance compared to those in direct contact. However, when an antenna is placed with a gap from the human body, changes in dielectric properties can cause wave reflections, leading to radiation in the direction opposite to the body. For applications requiring the sensing of body signals from an implantable device, a directly attached antenna is preferable.

K. ELECTROMAGNETIC SIMULATION TOOLS

Software Computer Simulation Technology (CST) *STUDIO*® is used to model and analyze antenna performance in virtual environments, allowing for optimization before physical prototyping.

VI. A NEW ANTENNA DESIGN FOR MEDICAL APPLICATIONS

A. ANTENNA DESIGN

The 3D geometry of the antenna design proposed for on–body and implantable medical applications is shown in Figure 7.

The proposed design is etched on a multilayer PCB with a layer–to–layer separation of 0.127 mm. The layer-wise geometry of the proposed design is shown in Figure 8.

The overall volume of the antenna is $7.7 \times 6 \times 0.359\ mm^3$ and is modeled for a 5.8 GHz ISM band. The dielectric properties of the skin, fat, and muscle layers are considered in simulations to mimic on–body placement. As the antenna design is small, it is impossible to use a standard SMA connector to feed the RF input. So, a coaxial probe feed is modeled in simulations. It can be seen from Figure 8

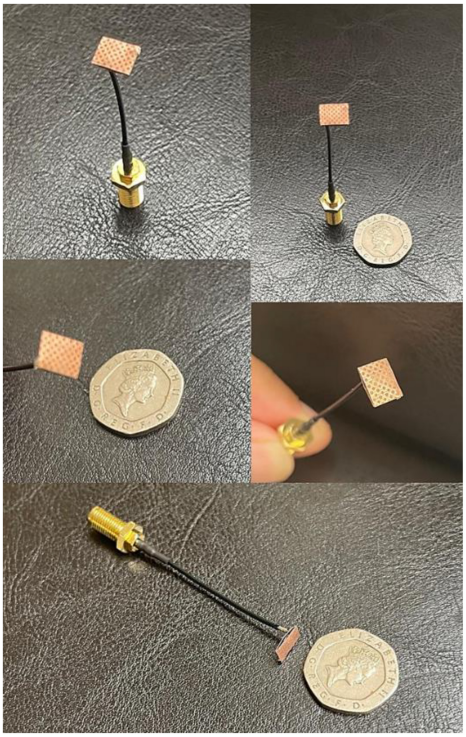

FIGURE 9. Fabricated prototype of the proposed antenna.

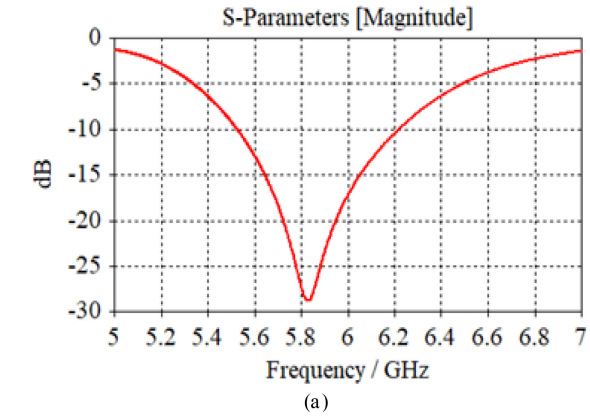

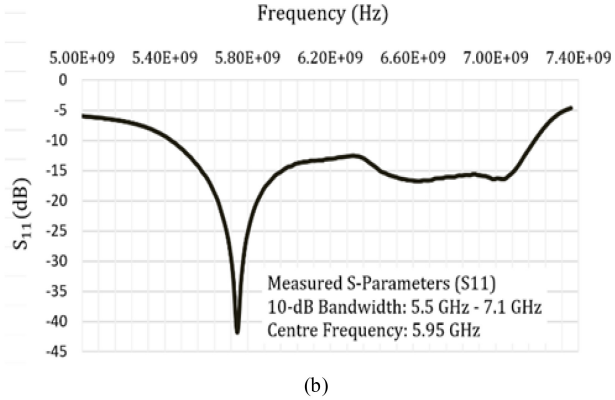

FIGURE 10. S_{11} of the Proposed Antenna for medical applications. (a): Simulated S_{11}. (b) Measured S_{11}.

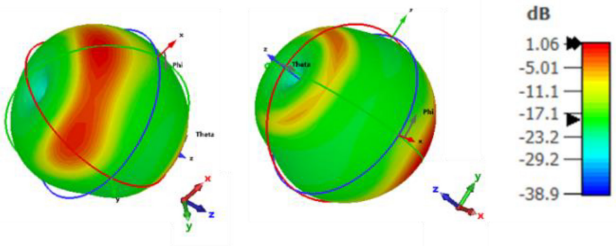

FIGURE 11. 3D Radiation pattern of the proposed Antenna for medical applications at 5.8 GHz.

that the design is etched on a three-layered Rogers RT–5880 substrate with a dielectric constant of 2.2. Layer 1 of the design comprises the ground plane of the design. Layer 2 is the main patch antenna. Layer 3 of the design is an EBG–inspired printed pattern which enhances the gain and efficiency of the antenna. The design consists of a slot that is etched in the ground plane and the patch for the enhancement of bandwidth. The design is formulated through an empirical approach, involving extensive simulations conducted on CST Microwave Studio® to determine the optimal dimensions. The design is miniature with an extremely small footprint which makes it suitable for modern medical on–body and implantable applications. The design is probe-fed which makes it suitable for on-body applications. However, the small size of the antenna makes it equally suitable for battery powered implantable applications. The shape and dimensions of the proposed antenna have evolved from rigorous simulation analyses that make its mathematical modeling and formulation complex or impossible. A fabricated prototype of the proposed antenna is shown in Figure 9.

B. RESULTS AND DISCUSSIONS

- *S–Parameters:* The simulated and measured S-parameters of the proposed antenna are shown in Figure 9. The S–parameters graph reveals that the antenna is radiating with a 10 dB return loss bandwidth of 500 MHz, ranging from approximately 5.7 to 6.2 GHz thereby covering the 5.8 GHz ISM frequency band completely. The simulated S11 was −30 dB at 5.8 GHz and −28 dB at 5.85 GHz in simulations whereas, the measured S_{11} showed a significant improvement, with a return loss of −43 dB at 5.8 GHz. This substantial enhancement in return loss indicates better impedance matching and reduced signal reflection in the fabricated antenna, confirming the reliability and robustness of the design. The overall bandwidth exhibits a value of return loss that depicts a good performance by the antenna. There is a slight discrepancy in the measurement results that occurred due to fabrication imperfections and the practical setup. The measured results were acquired by attaching the antenna to a human arm.

- *Radiation Pattern:* Simulated 3D radiation pattern of the proposed antenna at 5.8 GHz is shown in Figure 10.

The radiation pattern fairly resembles an Omni–directional pattern. A 2D view of the pattern is shown in Figure 11. The

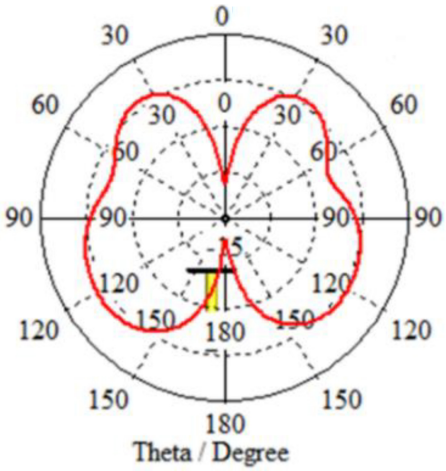

FIGURE 12. 2D Radiation Pattern (Theta Plane) of the Proposed Antenna for medical applications.

TABLE 7. Simulated gain and efficiency of the proposed antenna.

Freq. (GHz)	Approximate gain (dB)	Approximate Efficiency (%)
5.7	0.75	50.0
5.8	1.06	53.0
5.9	1.26	53.5
6.0	1.38	53.0
6.1	1.40	51.0
6.2	1.35	48.0

2D radiation pattern is shown with the antenna structure and is plotted in the theta plane. The antenna radiation increases from 0 to approximately 130 degrees. The maximum value of radiation occurs around 40 degrees whereas, the unwanted radiation along the feedline is minimum.

- *Gain and Efficiency:* The antenna gain, and efficiency are obtained from the simulations. The simulated results are presented in Table 7.

The realized gain of the antenna at 5.8 GHz is 1.06 dB whereas, the efficiency is around 53%. The design possesses good values of gain and efficiency in the entire bandwidth. This makes the design more suitable for on-body and implantable medical applications because these readings are obtained after considering the skin layers. The measurement results presented so far show minor discrepancies due to a more realistic practical setup including the connecting cables and real human arm.

C. SUMMARY

The presented results of the proposed antenna for medical applications are suitable for on-body direct contact applications. The design considers major practical constraints in the simulations which can ensure its good practical performance. The design is miniature with a very small size making it suitable for small medical sensors. A comparison between the proposed antenna and the key design from the review is shown in Table 1. It can be seen that the proposed antenna possesses excellent gain and efficiency performances as compared to the reviewed designs. Further testing will be conducted for practical validation of radiation parameters such as gain, efficiency, and radiation pattern. The detailed antenna design, parametric analysis, and results, including the simulations and measurements, will be presented and discussed in a separate manuscript.

VII. FUTURE RESEARCH DIRECTIONS IN MEDICAL ANTENNAS

Medical antennas, that involve the use of EM waves for medical applications, have seen significant progress in recent years [66], [67], [68], [69], [70], [71], [72], [73]. They have the potential to revolutionize the field of healthcare [74], [75], [76]. For the future, there are several promising research directions in medical antennas that could pave the way for groundbreaking discoveries and innovations [66], [67], [68], [69], [70], [71], [72], [73], [74], [75], [76].

A prospective research avenue in medical antennas involves the development of miniaturized antennas tailored for implantable medical devices. Despite the substantial advancements in devices like pacemakers, neurostimulators, and drug delivery systems that have significantly enhanced patient quality of life, the persistent challenge lies in the size and form factor of these implants. The exploration of miniaturized antennas, seamlessly integrated into these devices without compromising functionality or safety, holds the potential to unlock novel capabilities for remote monitoring, control, and communication. The integration of tiny antennas within implantable devices could usher in a new era of possibilities. For instance, these miniaturized antennas might facilitate wireless power transmission and communication with implanted devices, eliminating the necessity for invasive procedures such as battery replacements or adjustments. This advancement enhance patient comfort, reduce medical interventions, and contribute to the overall effectiveness of implantable medical devices [76], [77], [78].

Another captivating research direction involves leveraging advanced antenna technologies for wireless imaging and diagnostics in the medical field. Conventional medical imaging techniques, including X-rays, CT scans, and MRI, face challenges related to resolution, contrast, and safety [72], [73]. Exploring wireless imaging methods utilizing antennas, such as microwave or terahertz imaging, holds the potential to overcome these limitations. These techniques offer non–ionizing radiation, improved resolution, and the capability to penetrate tissues. Research in this domain could pave the way for the development of compact and portable wireless imaging devices. Such innovations may find applications in early cancer detection, monitoring chronic conditions, and providing real-time imaging during minimally invasive procedures. The integration of advanced antenna technologies into medical imaging holds promise for enhancing diagnostic capabilities, improving patient outcomes, and advancing the field of healthcare. Furthermore, there is a growing interest in using antennas for targeted and localized therapies. Antennas present an avenue for delivering therapeutic energy, such as

microwave or radiofrequency energy, to specific regions of the body for treatments like cancer ablation, hyperthermia, or neuromodulation. Nonetheless, current techniques encounter challenges related to precision, control, and safety. Future research endeavors could concentrate on advancing antenna designs and control algorithms to facilitate highly precise and customizable therapies. For instance, the exploration of phased array antennas, which permit dynamic and adaptable beam steering, holds the potential to enhance precision in targeting tumors or specific neural circuits. The development of such sophisticated technologies could revolutionize therapeutic approaches, offering improved efficacy and safety in localized treatments.

In addition, there is a pressing need for research in the realm of wireless communication within medical environments. Wireless communication assumes a pivotal role in numerous medical applications, including remote patient monitoring, telemedicine, and coordination among medical devices within hospital settings. However, medical environments are intricate and pose challenges due to the presence of diverse EM interference sources, stringent safety regulations, and privacy concerns. Future research endeavors could concentrate on the development of resilient and secure wireless communication techniques. These techniques should be designed to operate reliably in the complex and demanding context of medical environments while adhering to rigorous safety and privacy requirements. Addressing these challenges is paramount for ensuring the effectiveness, safety, and privacy of wireless communication in medical applications.

Finally, there is a burgeoning interest in integrating medical antennas with other emerging technologies, particularly artificial intelligence (AI), machine learning (ML), etc. AI/ML algorithms hold the potential to analyze data gathered from medical antennas, including EM signals or sensor data. This analysis can offer real-time feedback, make predictions, or optimize treatment plans. Concurrently, IoT technologies can facilitate seamless connectivity and interoperability among medical antennas, devices, and systems, ultimately contributing to enhanced patient care and outcomes. Future research endeavors may delve into the synergistic integration of medical antennas with AI and IoT, opening avenues for personalized medicine, remote healthcare, and intelligent healthcare systems. This convergence of technologies could usher in transformative possibilities, shaping the future landscape of healthcare delivery and patient well–being.

These advancements have the potential to revolutionize healthcare by enabling new diagnostic and therapeutic capabilities [66], [67], [68], [69], [70], [71], [72], [73], [74], [75], [76], [77], [78].

VIII. CONCLUSION

A comprehensive review of more than 60 research papers has been presented in this paper. The antennas discussed in this paper are designed for medical applications such as on–body wearable terminals, implantable capsules and other medical devices. Various parameters of the antennas were discussed including gain, efficiency, SAR, and operating frequency. It has been observed that the on–body and implantable antennas have very low values of gain and efficiency due to the presence of skin, fat, and muscle layers. Also, the input power is limited due to the standard SAR requirements. The majority of the designs are modeled at ISM 2.4 GHz frequency and the designs at millimeter wave frequencies are rare. This makes medical antennas an exciting topic to carry out further research, simulations, and modeling to find the practical suitability of the millimeter wave frequencies for medical antennas. Lastly, the design and simulation performance of a new antenna was also discussed in this paper. The proposed new design possesses excellent gain and efficiency performances. Also, the design is miniature with a size of few millimeters which makes it more suitable for small medical applications.

REFERENCES

[1] R. S. Alrawashdeh, Y. Huang, M. Kod, and A. A. B. Sajak, "A broadband flexible implantable loop antenna with complementary split ring resonators," *IEEE Antennas Wireless Propag. Lett.*, vol. 14, pp. 1506–1509, 2015, doi: 10.1109/LAWP.2015.2403952.

[2] Z. Xia et al., "A wideband circularly polarized implantable patch antenna for ISM band biomedical applications," *IEEE Trans. Antennas Propag.*, vol. 68, no. 3, pp. 2399–2404, Mar. 2020, doi: 10.1109/TAP.2019.2944538.

[3] K. M. Labus, B. M. Notaroš, M. M. Ilić, C. J. Sutherland, A. Holcomb, and C. M. Puttlitz, "A coaxial dipole antenna for passively sensing object displacement and deflection for orthopaedic applications," *IEEE Access*, vol. 6, pp. 68184–68194, 2018, doi: 10.1109/ACCESS.2018.2878904.

[4] Y. H. Jung et al., "A compact parylene-coated WLAN flexible antenna for implantable electronics," *IEEE Antennas Wireless Propag. Lett.*, vol. 15, pp. 1382–1385, 2016, doi: 10.1109/LAWP.2015.2510372.

[5] S. Das and D. Mitra, "A compact wideband flexible implantable slot antenna design with enhanced gain," *IEEE Trans. Antennas Propag.*, vol. 66, no. 8, pp. 4309–4314, Aug. 2018, doi: 10.1109/TAP.2018.2836463.

[6] A. Sharma, E. Kampianakis, and M. S. Reynolds, "A dual-band HF and UHF antenna system for implanted neural recording and stimulation devices," *IEEE Antennas Wireless Propag. Lett.*, vol. 16, pp. 493–496, 2017, doi: 10.1109/LAWP.2016.2585650.

[7] S. Bakogianni and S. Koulouridis, "A dual-band implantable rectenna for wireless data and power support at sub-GHz region," *IEEE Trans. Antennas Propag.*, vol. 67, no. 11, pp. 6800–6810, Nov. 2019, doi: 10.1109/TAP.2019.2927879.

[8] M. Song et al., "A millimeter-scale crystal-less MICS transceiver for insertable smart pills," *IEEE Trans. Biomed. Circuits Syst.*, vol. 14, no. 6, pp. 1218–1229, Dec. 2020, doi: 10.1109/TBCAS.2020.3036905.

[9] H. Li, Y.-X. Guo, C. Liu, S. Xiao, and L. Li, "A miniature-implantable antenna for medradio-band biomedical telemetry," *IEEE Antennas Wireless Propag. Lett.*, vol. 14, pp. 1176–1179, 2015, doi: 10.1109/LAWP.2015.2396535.

[10] R. Li, Y.-X. Guo, B. Zhang, and G. Du, "A miniaturized circularly polarized implantable annular-ring antenna," *IEEE Antennas Wireless Propag. Lett.*, vol. 16, pp. 2566–2569, 2017, doi: 10.1109/LAWP.2017.2734246.

[11] X. Y. Liu, Z. T. Wu, Y. Fan, and E. M. Tentzeris, "A miniaturized CSRR loaded wide-beamwidth circularly polarized implantable antenna for subcutaneous real-time glucose monitoring," *IEEE Antennas Wireless Propag. Lett.*, vol. 16, pp. 577–580, 2017, doi: 10.1109/LAWP.2016.2590477.

[12] F. Faisal, M. Zada, A. Ejaz, Y. Amin, S. Ullah, and H. Yoo, "A miniaturized dual-band implantable antenna system for medical applications," *IEEE Trans. Antennas Propag.*, vol. 68, no. 2, pp. 1161–1165, Feb. 2020, doi: 10.1109/TAP.2019.2938591.

[13] Y. Fan, J. Huang, T. Chang, and X. Liu, "A miniaturized four-element MIMO antenna with EBG for implantable medical devices," *IEEE J. Electromagn., RF, Microw. Med. Biol.*, vol. 2, no. 4, pp. 226–233, Dec. 2018, doi: 10.1109/JERM.2018.2871458.

[14] F. Faisal and H. Yoo, "A miniaturized novel-shape dual-band antenna for implantable applications," *IEEE Trans. Antennas Propag.*, vol. 67, no. 2, pp. 774–783, Feb. 2019, doi: 10.1109/TAP.2018.2880046.

[15] M. Zada and H. Yoo, "A miniaturized triple-band implantable antenna system for bio-telemetry applications," *IEEE Trans. Antennas Propag.*, vol. 66, no. 12, pp. 7378–7382, Dec. 2018, doi: 10.1109/TAP.2018.2874681.

[16] A. Abdi and H. Aliakbarian, "A miniaturized UHF-band rectenna for power transmission to deep-body implantable devices," *IEEE J. Transl. Eng. Health Med.*, vol. 7, 2019, Art no. 1900311, doi: 10.1109/JTEHM.2019.2910102.

[17] R. S. Hassan, J. Lee, and S. Kim, "A minimally invasive implantable sensor for continuous wireless glucose monitoring based on a passive resonator," *IEEE Antennas Wireless Propag. Lett.*, vol. 19, no. 1, pp. 124–128, Jan. 2020, doi: 10.1109/LAWP.2019.2955176.

[18] Y. Liu, Y. Chen, H. Lin, and F. H. Juwono, "A novel differentially fed compact dual-band implantable antenna for biotelemetry applications," *IEEE Antennas Wireless Propag. Lett.*, vol. 15, pp. 1791–1794, 2016, doi: 10.1109/LAWP.2016.2536735.

[19] S. M. Asif, A. Iftikhar, J. W. Hansen, M. S. Khan, D. L. Ewert, and B. D. Braaten, "A Novel RF-powered wireless pacing via a rectenna-based pacemaker and a wearable transmit-antenna array," *IEEE Access*, vol. 7, pp. 1139–1148, 2019, doi: 10.1109/ACCESS.2018.2885620.

[20] A. Basir and H. Yoo, "A stable impedance-matched ultrawideband antenna system mitigating detuning effects for multiple biotelemetric applications," *IEEE Trans. Antennas Propag.*, vol. 67, no. 5, pp. 3416–3421, May 2019, doi: 10.1109/TAP.2019.2905891.

[21] Y. Zhang, C. Liu, X. Liu, K. Zhang, and X. Yang, "A wide-band circularly polarized implantable antenna for 915 MHzISM-band biotelemetry devices," *IEEE Antennas Wireless Propag. Lett.*, vol. 17, no. 8, pp. 1473–1477, Aug. 2018, doi: 10.1109/LAWP.2018.2849847.

[22] S. M. Asif, A. Iftikhar, B. D. Braaten, D. L. Ewert, and K. Maile, "A wide-band tissue numerical model for deeply implantable antennas for RF-powered leadless pacemakers," *IEEE Access*, vol. 7, pp. 31031–31042, 2019, doi: 10.1109/ACCESS.2019.2902981.

[23] J. Wang, M. Leach, E. G. Lim, Z. Wang, R. Pei, and Y. Huang, "An implantable and conformal antenna for wireless capsule endoscopy," *IEEE Antennas Wireless Propag. Lett.*, vol. 17, no. 7, pp. 1153–1157, Jul. 2018, doi: 10.1109/LAWP.2018.2836392.

[24] Y. Li, L. Yang, W. Duan, and X. Zhao, "An implantable antenna design for an intelligent health monitoring system considering the relative permittivity and conductivity of the human body," *IEEE Access*, vol. 7, pp. 38236–38244, 2019, doi: 10.1109/ACCESS.2019.2899242.

[25] B. Rana, J.-Y. Shim, and J.-Y. Chung, "An implantable antenna with broadside radiation for a brain-machine interface," *IEEE Sensors J.*, vol. 19, no. 20, pp. 9200–9205, Oct. 2019, doi: 10.1109/JSEN.2019.2924948.

[26] Z.-J. Yang, L. Zhu, and S. Xiao, "An implantable circularly polarized patch antenna design for pacemaker monitoring based on quality factor analysis," *IEEE Trans. Antennas Propag.*, vol. 66, no. 10, pp. 5180–5192, Oct. 2018, doi: 10.1109/TAP.2018.2862242.

[27] S. Bakogianni and S. Koulouridis, "An implantable planar dipole antenna for wireless MedRadio-band biotelemetry devices," *IEEE Antennas Wireless Propag. Lett.*, vol. 15, pp. 234–237, 2016, doi: 10.1109/LAWP.2015.2439039.

[28] Z.-J. Yang, L. Zhu, and S. Xiao, "An implantable wideband circularly polarized microstrip patch antenna via two pairs of degenerate modes," *IEEE Access*, vol. 7, pp. 4239–4247, 2019, doi: 10.1109/ACCESS.2018.2887234.

[29] Z.-J. Yang, L. Zhu, and S. Xiao, "An implantable wide-band microstrip patch antenna based on high-loss property of human tissue," *IEEE Access*, vol. 8, pp. 93048–93057, 2020, doi: 10.1109/ACCESS.2020.2994358.

[30] M. Berg, J. Chen, and A. Pärssinen, "Analysis of vertical loop antenna and its wide and flat variant performance in wearable use," *IEEE Access*, vol. 6, pp. 22570–22577, 2018, doi: 10.1109/ACCESS.2018.2824542.

[31] L.-J. Xu, Y.-X. Guo, and W. Wu, "Bandwidth enhancement of an implantable antenna," *IEEE Antennas Wireless Propag. Lett.*, vol. 14, pp. 1510–1513, 2015, doi: 10.1109/LAWP.2014.2374217.

[32] L.-J. Xu, Y. Bo, W.-J. Lu, L. Zhu, and C.-F. Guo, "Circularly polarized annular ring antenna with wide axial-ratio bandwidth for biomedical applications," *IEEE Access*, vol. 7, pp. 59999–60009, 2019, doi: 10.1109/ACCESS.2019.2915236.

[33] C. Liu, Y. Zhang, and X. Liu, "Circularly polarized implantable antenna for 915 MHzISM-band far-field wireless power transmission," *IEEE Antennas Wireless Propag. Lett.*, vol. 17, no. 3, pp. 373–376, Mar. 2018, doi: 10.1109/LAWP.2018.2790418.

[34] L.-J. Xu, J.-P. Xu, Z.-J. Chu, S. Liu, and X. Zhu, "Circularly polarized implantable antenna with improved impedance matching," *IEEE Antennas Wireless Propag. Lett.*, vol. 19, no. 5, pp. 876–880, May 2020, doi: 10.1109/LAWP.2020.2983216.

[35] M. Manoufali, K. Bialkowski, B. Mohammed, P. C. Mills, and A. M. Abbosh, "Compact implantable antennas for cerebrospinal fluid monitoring," *IEEE Trans. Antennas Propag.*, vol. 67, no. 8, pp. 4955–4967, Aug. 2019, doi: 10.1109/TAP.2019.2896722.

[36] M. Yousaf et al., "Compacted conformal implantable antenna with multitasking capabilities for ingestible capsule endoscope," *IEEE Access*, vol. 8, pp. 157617–157627, 2020, doi: 10.1109/ACCESS.2020.3019663.

[37] A. Shah, M. Zada, and H. Yoo, "Design and analysis of a compact-sized multiband spiral-shaped implantable antenna for scalp implantable and leadless pacemaker systems," *IEEE Trans. Antennas Propag.*, vol. 67, no. 6, pp. 4230–4234, Jun. 2019, doi: 10.1109/TAP.2019.2908252.

[38] P. Anacleto, H. Dinis, J. Fernandes, and P. M. Mendes, "Design and characterization of 3-D self-folded microantennas for implantable microdevices," *IEEE Trans. Antennas Propag.*, vol. 68, no. 3, pp. 2031–2039, Mar. 2020, doi: 10.1109/TAP.2019.2948741.

[39] S. Hout and J.-Y. Chung, "Design and characterization of a miniaturized implantable antenna in a seven-layer brain phantom," *IEEE Access*, vol. 7, pp. 162062–162069, 2019, doi: 10.1109/ACCESS.2019.2951489.

[40] W. Lei, H. Chu, and Y.-X. Guo, "Design of a circularly polarized ground radiation antenna for biomedical applications," *IEEE Trans. Antennas Propag.*, vol. 64, no. 6, pp. 2535–2540, Jun. 2016, doi: 10.1109/TAP.2016.2552551.

[41] N. Ganeshwaran, J. K. Jeyaprakash, M. G. N. Alsath, and V. Sathyanarayanan, "Design of a dual-band circular implantable antenna for biomedical applications," *IEEE Antennas Wireless Propag. Lett.*, vol. 19, no. 1, pp. 119–123, Jan. 2020, doi: 10.1109/LAWP.2019.2955140.

[42] W. Cui, R. Liu, L. Wang, M. Wang, H. Zheng, and E. Li, "Design of wideband implantable antenna for wireless capsule endoscope system," *IEEE Antennas Wireless Propag. Lett.*, vol. 18, no. 12, pp. 2706–2710, Dec. 2019, doi: 10.1109/LAWP.2019.2949630.

[43] D. Nikolayev, W. Joseph, A. Skrivervik, M. Zhadobov, L. Martens, and R. Sauleau, "Dielectric-loaded conformal microstrip antennas for versatile in-body applications," *IEEE Antennas Wireless Propag. Lett.*, vol. 18, no. 12, pp. 2686–2690, Dec. 2019, doi: 10.1109/LAWP.2019.2948814.

[44] G. Samanta and D. Mitra, "Dual-band circular polarized flexible implantable antenna using reactive impedance substrate," *IEEE Trans. Antennas Propag.*, vol. 67, no. 6, pp. 4218–4223, Jun. 2019, doi: 10.1109/TAP.2019.2905978.

[45] J. M. Felício, J. R. Costa, and C. A. Fernandes, "Dual–band skin-adhesive repeater antenna for continuous body signals monitoring," *IEEE J. Electromagn., RF, Microw. Med. Biol.*, vol. 2, no. 1, pp. 25–32, Mar. 2018, doi: 10.1109/JERM.2018.2806186.

[46] M. Chrysler, C. M. Furse, K. L. Hall, and Y. Chung, "Effect of material properties on a subdermal UHF RFID antenna," *IEEE J. Radio Freq. Identif.*, vol. 1, no. 4, pp. 260–266, Dec. 2017, doi: 10.1109/JRFID.2018.2791919.

[47] A. Basir and H. Yoo, "Efficient wireless power transfer system with a miniaturized quad-band implantable antenna for deep-body multitasking implants," *IEEE Trans. Microw. Theory Techn.*, vol. 68, no. 5, pp. 1943–1953, May 2020, doi: 10.1109/TMTT.2020.2965938.

[48] H. Bahrami, S. A. Mirbozorgi, R. Ameli, L. A. Rusch, and B. Gosselin, "Flexible, polarization-diverse UWB antennas for implantable neural recording systems," *IEEE Trans. Biomed. Circuits Syst.*, vol. 10, no. 1, pp. 38–48, Feb. 2016, doi: 10.1109/TBCAS.2015.2393878.

[49] Y.-S. Jou, R. Azadegan, and S. Mohammadi, "High-resistivity CMOS SOI rectenna for implantable applications," *IEEE Microw. Wireless Compon. Lett.*, vol. 27, no. 9, pp. 854–856, Sep. 2017, doi: 10.1109/LMWC.2017.2734776.

[50] C.-L. Tsai, K.-W. Chen, and C.-L. Yang, "Implantable wide-band low-SAR Antenna with C-shaped coupled ground," *IEEE Antennas Wireless Propag. Lett.*, vol. 14, pp. 1594–1597, 2015, doi: 10.1109/LAWP.2015.2413839.

[51] S. Ding, S. Koulouridis, and L. Pichon, "Implantable wireless transmission rectenna system for biomedical wireless applications," *IEEE Access*, vol. 8, pp. 195551–195558, 2020, doi: 10.1109/ACCESS.2020.3032848.

[52] J. Blauert, Y.-S. Kang, and A. Kiourti, "In Vivo Testing of a miniature 2.4/4.8 GHz implantable antenna in postmortem human subject," *IEEE Antennas Wireless Propag. Lett.*, vol. 17, no. 12, pp. 2334–2338, Dec. 2018, doi: 10.1109/LAWP.2018.2874099.

[53] C. Liu, Y.-X. Guo, R. Jegadeesan, and S. Xiao, "In Vivo testing of circularly polarized implantable antennas in rats," *IEEE Antennas Wireless Propag. Lett.*, vol. 14, pp. 783–786, 2015, doi: 10.1109/LAWP.2014.2382559.

[54] Z. Duan, L.-J. Xu, S. Gao, and W. Geyi, "Integrated design of wide-band omnidirectional antenna and electronic components for wireless capsule endoscopy systems," *IEEE Access*, vol. 6, pp. 29626–29636, 2018, doi: 10.1109/ACCESS.2018.2840689.

[55] K. N. Ketavath, D. Gopi, and S. Sandhya Rani, "In-vitro test of miniaturized CPW-fed implantable conformal patch antenna at ISM band for biomedical applications," *IEEE Access*, vol. 7, pp. 43547–43554, 2019, doi: 10.1109/ACCESS.2019.2905661.

[56] M. Zada, I. A. Shah, and H. Yoo, "Metamaterial-loaded compact high-gain dual-band circularly polarized implantable antenna system for multiple biomedical applications," *IEEE Trans. Antennas Propag.*, vol. 68, no. 2, pp. 1140–1144, Feb. 2020, doi: 10.1109/TAP.2019.2938573.

[57] L.-J. Xu, Y.-X. Guo, and W. Wu, "Miniaturized circularly polarized loop antenna for biomedical applications," *IEEE Trans. Antennas Propag.*, vol. 63, no. 3, pp. 922–930, Mar. 2015, doi: 10.1109/TAP.2014.2387420.

[58] I. Gani and H. Yoo, "Multi-band antenna system for skin implant," *IEEE Microw. Wireless Compon. Lett.*, vol. 26, no. 4, pp. 294–296, Apr. 2016, doi: 10.1109/LMWC.2016.2538470.

[59] H. Wong, W. Lin, L. Huitema, and E. Arnaud, "Multi-polarization reconfigurable antenna for wireless biomedical system," *IEEE Trans. Biomed. Circuits Syst.*, vol. 11, no. 3, pp. 652–660, June 2017, doi: 10.1109/TBCAS.2016.2636872.

[60] A. Valanarasi and R. Dhanasekaran, "Optimum band ε shaped miniature implantable antennas for telemetry applications," *IEEE Trans. Antennas Propag.*, vol. 69, no. 1, pp. 55–63, Jan. 2021, doi: 10.1109/TAP.2020.3008622.

[61] X.-T. Yang, H. Wong, and J. Xiang, "Polarization reconfigurable planar inverted-F antenna for implantable telemetry applications," *IEEE Access*, vol. 7, pp. 141900–141909, 2019, doi: 10.1109/ACCESS.2019.2941388.

[62] V. T. Nguyen and C. W. Jung, "Radiation-pattern reconfigurable antenna for medical implants in MedRadio band," *IEEE Antennas Wireless Propag. Lett.*, vol. 15, pp. 106–109, 2016, doi: 10.1109/LAWP.2015.2432172.

[63] L.-J. Xu, X. Jin, D. Hua, W.-J. Lu, and Z. Duan, "Realization of circular polarization and gain enhancement for implantable antenna," *IEEE Access*, vol. 8, pp. 16857–16864, 2020, doi: 10.1109/ACCESS.2019.2963744.

[64] "IEEE Standards Association," Accessed: Apr. 19, 2023. [Online]. Available: https://standards.ieee.org/ieee/62704–4/10555/

[65] "National radio research agency," Rra.go.kr, 2018. Accessed : Apr. 19, 2023. [Online]. Available: https://www.rra.go.kr/en/sar/standard.do

[66] C. M. Furse and A. Chrysler, "A history & future of implantable antennas," in *Proc. IEEE Antennas Propag. Soc. Int. Symp. (APSURSI)*, Memphis, TN, USA, 2014, pp. 527–528, doi: 10.1109/APS.2014.6904595.

[67] S. A. A. Shah, Y.-H. Lim, and H. Yoo, "A novel development of endovascular aortic stent system featuring promising antenna characteristics," *IEEE Trans. Antennas Propag.*, vol. 70, no. 3, pp. 2214–2222, Mar. 2022, doi: 10.1109/TAP.2021.3111200.

[68] E. Topsakal, "Wireless medical telemetry: Current status and future directions," *in Proc. USNC–URSI Radio Sci. Meeting (Joint With AP-S Symposium)*, Memphis, TN, USA, 2014, pp. 244–244, doi: 10.1109/USNC–URSI.2014.6955627.

[69] K. Ito, "Keynote speech 3: Recent medical applications of electromagnetic waves," in *Proc. Int. Workshop Electromagn. Appl. Student Innov. Compet.*, London, U.K., 2017, pp. 1–5, doi: 10.1109/iWEM.2017.7968793.

[70] S. A. A. Shah, I. A. Shah, S. Hayat, and H. Yoo, "Ultra-miniaturized implantable antenna enabling multiband operation for diverse industrial IoMT devices," *IEEE Trans. Antennas Propag.*, vol. 72, no. 2, pp. 1352–1362, Feb. 2024, doi: 10.1109/TAP.2024.3349782.

[71] N. A. Kamaruddin, S. N. Azemi, S. Z. Ibrahim, A. A. H. Azremi, and N. F. Kahar, "Antenna for in–body communications," in *Proc. IEEE Asia–Pacific Conf. Appl. Electromagn. (APACE)*, Melacca, Malaysia, 2019, pp. 1–6, doi: 10.1109/APACE47377.2019.9020955.

[72] J.-C. Bolomey and L. Jofre, "Three decades of active microwave imaging achievements, difficulties and future challenges," in *Proc. IEEE Int. Conf. Wireless Inf. Technol. Syst.*, Honolulu, HI, USA, 2010, pp. 1–4, doi: 10.1109/ICWITS.2010.5611904.

[73] R. Chandra, H. Zhou, I. Balasingham, and R. M. Narayanan, "On the opportunities and challenges in microwave medical sensing and imaging," *IEEE Trans. Biomed. Eng.*, vol. 62, no. 7, pp. 1667–1682, Jul. 2015, doi: 10.1109/TBME.2015.2432137.

[74] S. A. A. Shah, A. Basir, Y.-H. Lim, and H. Yoo, "A novel efficient wirelessly powered biotelemetric endovascular aortic stent antenna system," *IEEE Trans. Antennas Propag.*, vol. 71, no. 9, pp. 7132–7145, Sep. 2023, doi: 10.1109/TAP.2023.3291419.

[75] Q. H. Abbasi et al., "Nano-communication for biomedical applications: A review on the state-of-the-art from physical layers to novel networking concepts," *IEEE Access*, vol. 4, pp. 3920–3935, 2016, doi: 10.1109/ACCESS.2016.2593582.

[76] A. Kiourti and K. S. Nikita, "Recent advances in implantable antennas for medical telemetry [education column]," *IEEE Antennas Propag. Mag.*, vol. 54, no. 6, pp. 190–199, Dec. 2012, doi: 10.1109/MAP.2012.6387813.

[77] R. Y. Khattak, Q. Z. Ahmed, S. Shoaib, and M. Hafeez, "Array antenna for wireless access points and futuristic healthcare devices," *Electronics*, vol. 11, no. 8, p. 1226, 2022. [Online]. Available: https://doi.org/10.3390/electronics11081226

[78] S. A. A. Shah and H. Yoo, "Scalp-implantable antenna systems for intracranial pressure monitoring," *IEEE Trans. Antennas Propag.*, vol. 66, no. 4, pp. 2170–2173, Apr. 2018, doi: 10.1109/TAP.2018.2801346.

RIQZA Y. KHATTAK (Student Member, IEEE) received the bachelor's degree in electrical and electronic engineering from COMSATS University, Abbottabad, Pakistan, in 2015, and the master's degree in electrical engineering from HITEC University, Taxila, Pakistan, in 2019. She is currently pursuing the Ph.D. degree with the University of Huddersfield, U.K., where she focuses on the design, optimization, and testing of antennas for implantable and wearable medical devices.

QASIM Z. AHMED (Member, IEEE) is currently a Reader of Electronic Engineering with the School of Computing and Engineering, University of Huddersfield, U.K., in 2017, 2018, and 2020, respectively. His research interests include mainly ultrawide bandwidth systems, millimeter waves, device to device, digital health, and cooperative communications. He is currently a Principal Investigator, U.K. for Erasmus + Digi Health-Asia project and the MSCA Staff Exchanges EVOLVE Project. He is a Co-Investigator of EU H2020 ETN Research MOTOR5G Project and EU H2020 RISE Research RECOMBINE Project. He is a Fellow of HEA.

SULTAN SHOAIB (Senior Member, IEEE) received the B.Sc. degree from the Institute of Space Technology, Islamabad, Pakistan, in 2010, and the Ph.D. degree in electronic engineering from the Queen Mary University of London in 2016. He is a Senior Lecturer (Associate Professor) with Wrexham University, Wrexham, U.K. With over 15 years of experience, he has been actively engaged in the design and testing of antennas and RF devices for a wide range of applications, including medical antennas and millimeter-wave communications.

PAVLOS I. LAZARIDIS (Senior Member, IEEE) is currently a Professor of Electronics and Telecommunications with the University of Huddersfield, U.K. He has been involved as a Principal Investigator in several international research projects, such as EU Horizon 2020 MOTOR5G, RECOMBINE, Horizon Europe 6G-ICARUS, and ISAC Newton. He has published over 200 research articles and several national and European patents. He is serving as an Associate Editor for IEEE ACCESS. He is a member of IET, a Senior Member of URSI, and a Fellow of the Higher Education Academy.

TEMITOPE T. ALADE received the B.Sc. degree in computer science from the University of Ilorin in 2003, the M.Sc. degree in mobile computing from the University of Bradford in 2007, and the Ph.D. degree in electronic engineering from the University of Kent in 2012. He is currently an Associate Professor of Computing Sciences with the School of Computing Sciences, University of East Anglia. From June 2020 to December 2022, he was a Senior Lecturer of Computer Science with Nottingham Trent University, where he was the Course Leader for M.Sc. Computer Science, and the M.Sc. Research Project Coordinator. From September 2016 to May 2020, he was a Senior Lecturer of Computing with the Department of Computing, University of Worcester, where he was the Research Excellence Framework Coordinator and a Research Group Coordinator for the Applied Computing Research Group. From September 2015 to August 2016, he was a Teaching Fellow of Computing with the School of Computing and Mathematics, University of Keele. From June 2012 to September 2015, he worked as a Postdoctoral Research Associate and then as a Lecturer of Mobile Communication with the University of Kent. His research interests include modeling and analysis of computing and communication systems, such as those found in mobile communication systems, mobile computing systems, Web-based systems, Internet of Things, machine learning and their applications in every area of public life including, finance, healthcare, wireless networks, buildings, entertainment, and related industries. His research spans the whole spectrum from technical design, through algorithms to system development and performance evaluation.